

Dear Editor,

Thank you for the comments which are helpful for us to further improve our manuscript.

Accompanying this letter, please find the revised manuscript entitled “Impact of assimilating a merged sea ice thickness from CryoSat-2 and SMOS in the Arctic reanalysis” for consideration of publication as an article in the Cryosphere.

The main modifications in the revision are listed below:

- We have improved the English as recommendation (not Abstract alone).
- Correct Eq. (5) and cut some duplicates as well.
- Complement an explanation for “superobed”.

Also as the requirement, the responses are listed as follow one by one: the comments are in black and our response in red.

I am generally satisfied with the responses to the reviewers and the changes made to the manuscript. The only issue that remains is that the wording is awkward in many places. The abstract in particular could benefit from rewriting for clarity and better wording. I don't know if you can solicit the help of a native english speaker, but I would suggest more careful editing.

-A: Thank you for this point. The Abstract part has been rewritten partly, and the rest parts (mostly in the Sections of Introduction, 2 and 3) have been polished again (see the revision).

In addition, where does the word superobed come from? Is that a scientific term? If the word is not necessary, I would suggest removing it.

-A: Yes. The superob procedure was initially applied for quality control to the noised observations before data assimilation (see Lorenc, 1981; Phoebus, 1990). At present, it becomes a widely accepted concept for data assimilation community of both atmosphere (Kazumori, 2014) and ocean (Keppenne and Rienecker, 2002;).

Lorenc, A.C. (1981): [A Global Three-Dimensional Multivariate Statistical Interpolation Scheme](https://doi.org/10.1175/1520-0493(1981)109<0701:AGTDMS>2.0.CO;2). *Mon. Wea. Rev.*, **109**, 701–721, [https://doi.org/10.1175/1520-0493\(1981\)109<0701:AGTDMS>2.0.CO;2](https://doi.org/10.1175/1520-0493(1981)109<0701:AGTDMS>2.0.CO;2)

Phoebus, P. A. (1990): Quality control algorithms for ocean temperature data, Naval Ocean Research and Development Activity, Report 243, March 1990 (<http://www.dtic.mil/dtic/tr/fulltext/u2/a229984.pdf>).

Kazumori, M. (2014): [Satellite Radiance Assimilation in the JMA Operational Mesoscale 4DVAR System](https://doi.org/10.1175/MWR-D-13-00135.1). *Mon. Wea. Rev.*, **142**, 1361–1381, <https://doi.org/10.1175/MWR-D-13-00135.1>

Keppenne, C.L. and M.M. Rienecker (2002): [Initial Testing of a Massively Parallel Ensemble Kalman Filter with the Poseidon Isopycnal Ocean General Circulation Model](https://doi.org/10.1175/1520-0493(2002)130<2951:ITOAMP>2.0.CO;2). *Mon. Wea. Rev.*, **130**, 2951–2965, [https://doi.org/10.1175/1520-0493\(2002\)130<2951:ITOAMP>2.0.CO;2](https://doi.org/10.1175/1520-0493(2002)130<2951:ITOAMP>2.0.CO;2)

So see in the revision P8 L225-227:

“... “superobed”: all observations falling within the same grid cell are averaged and the observation uncertainty is reduced accordingly (Sakov et al., 2012).”

1
2
3
4
5
6
7
8
9
10
11
12
13
14
15
16
17
18
19
20
21
22
23

Impact of assimilating a merged sea ice thickness from CryoSat-2 and SMOS in the Arctic reanalysis

Jiping Xie¹, François Counillon^{1,2}, and Laurent Bertino^{1,2}

1. *Nansen Environmental and Remote Sensing Center, Bergen N5006, Norway*
2. *Bjerknes Center for Climate Research, Bergen, Norway*

Formatted: Font: (Default) Arial, (Asian) Arial, Italic, Font color: Text 1

Formatted: Font: (Default) Arial, (Asian) Arial, Italic, Font color: Text 1

*Corresponding author: Jiping Xie, E-mail: jiping.xie@nersc.no

24

Abstract

25 ~~Forecasting accurately the~~ Sea Ice Thickness (SIT) ~~in the Arctic is~~ a major
 26 challenge. The new SIT ~~product (referred to as CS2SMOS)~~ merges
 27 measurements from the CryoSat-2 and SMOS satellites ~~on a weekly basis~~
 28 ~~during the winter~~. The impact of assimilating CS2SMOS ~~data~~ is tested for the
 29 TOPAZ4 system - the Arctic component of the Copernicus Marine Environment
 30 Monitoring Services (CMEMS). TOPAZ4 currently assimilates a large set of
 31 ocean and sea ice observations with the Deterministic Ensemble Kalman Filter
 32 (DEnKF).

- Deleted: Accurate
- Deleted: forecast of
- Deleted: represent
- Deleted: for Arctic forecasting systems
- Deleted: CS2SMOS
- Deleted: measurements
- Deleted: are available
- Deleted: during the winter months since October 2010

33 Two parallel reanalyses are conducted without (Official run) and with (Test run)
 34 assimilation of CS2SMOS ~~data~~ from 19th March 2014 to 31st March 2015. ~~Since~~
 35 ~~only mapping errors were provided in the CS2SMOS observation, an arbitrary~~
 36 ~~term was added to compensate for the missing errors, but~~ was found a
 37 posteriori ~~too large~~. The SIT bias (too thin) is reduced from 16 cm to 5 cm and
 38 the ~~standard errors decrease from 53 cm to 38 cm (by 28%)~~ when compared
 39 to the ~~assimilated SIT~~. When compared to independent SIT observations, the
 40 ~~error reduction is 24% against the Ice Mass Balance (IMB) buoy 2013F and by~~
 41 12.5% against SIT data from the IceBridge campaigns. ~~The improvement of~~
 42 ~~sea ice volume persists through the summer months in the absence of~~
 43 ~~CS2SMOS data. Comparisons to sea ice drift from satellite show that dynamical~~
 44 ~~adjustments reduce the drift errors around the North pole by about 8-9% in~~
 45 ~~December 2014 and February 2015~~. Finally, using the Degrees of Freedom for
 46 Signal (DFS), we find that CS2SMOS ~~makes the prime~~ source of information in
 47 the central Arctic and in the Kara Sea. ~~We therefore recommend the~~
 48 ~~assimilation of CS2SMOS for~~ Arctic reanalyses in order to improve the ice
 49 thickness and the ice drift.

- Deleted: the previously weekly
- Deleted: for the period
- Deleted: . A
- Deleted: added to compensate for the estimation, but i
- Deleted: reduction
- Deleted: simultaneous
- Deleted: from CS2SMOS
- Deleted: are reduced by
- Deleted: When compared to the satellite ice drift product, the RMSDs around the North pole are reduced by about 8-9% in December 2014 and February 2015 relative to that in the Official. Tgood improvement outside of the assimilation period
- Formatted: Font: (Default) Arial, (Asian) Arial, 12 pt, Font color: Text 1

50 **Keywords:** Sea ice thickness; Arctic reanalysis; CS2SMOS; EnKF; ~~observing~~
 51 ~~systems~~ evaluation;

- Deleted: is
- Formatted: Font: (Default) Arial, (Asian) Arial, 12 pt, Font color: Text 1
- Deleted: the
- Deleted: main
- Deleted: s
- Formatted: Font: (Default) Arial, (Asian) Arial, 12 pt, Font color: Text 1, English (UK)
- Deleted: These results suggest that CS2SMOS
- Deleted: should be includ
- Deleted: ed
- Deleted: in
- Deleted: ; Innovation
- Deleted: mpact

52
53

1. Introduction

Sea ice plays an important role in the Arctic climate system because it prevents the rapid exchange of heat flux between the ocean and atmosphere. A decline and a thinning of the sea ice cover has occurred in the past decades (e.g. Johannessen et al., 1999; Comiso et al., 2008; Stroeve et al., 2012), as well as an increase of deformation rates and drift speed (Rampal et al. 2009). It is expected that these changes will have significant impacts on the Arctic Ocean Circulation (e.g. Levermann et al., 2007; Budikova, 2009; Kinnard et al., 2011) and on the future human living environment (Schofield et al., 2011; Bathiany et al., 2016). The interpretation of such changes is severely hampered by the sparseness of observations, therefore the reanalyses that can provide continuous spatio-temporal reconstructions by assimilating existing observations into dynamical models have become increasingly popular tools. In addition, recent studies (Day et al. 2014; Guemas et al., 2014; Melia et al. 2015) have shown that SIT anomalies play an important role for the Arctic predictability up to seasonal time scale. Satellite observations of sea ice concentration (SIC) have been available since 1979 and have allowed an accurate monitoring of sea ice extent (SIE) during that period. Data assimilation of SIC has constrained the position of the sea ice edge (Lisæter et al., 2003; Stark et al., 2008; Posey et al., 2015), but large disagreements (e.g., Uotila et al, 2018) remain in the estimation of sea ice volume because observations of sea ice thickness (SIT) are very incomplete. Until the 1990s, the only SIT measurements were sparse in situ measurements and submarine data. With new satellites, continuous estimates of SIT on basin scale have been achieved using satellite radar and laser altimeters; European Remote Sensing (ERS), Envisat and the NASA Ice, Cloud and land Elevation Satellite (ICESat). These were used to document the rapid thinning of sea ice in Arctic (Laxon et al., 2003; Kwok and Rothrock, 2009). CryoSat-2, launched in April 2010, has been the first satellite dedicated to measure with high accuracy the sea ice freeboard, from which SIT can be derived (Ricker et al., 2014; Tilling et al., 2016). However, the resulting SIT estimates are still very uncertain because of uncertainties in the snow depth (using climatology), snow penetration and sea ice density (Kern et al, 2015; Khvorostovsky and Rampal, 2016). Those uncertainties are large for thin ice

Formatted: List Paragraph, Justified, Line spacing: 1,5 lines

Formatted: Font: (Default) Arial, (Asian) Arial, 12 pt, Font color: Text 1, (Asian) Chinese (China)

Deleted: i

Deleted: use of

Deleted: s

Formatted: Font: (Default) Arial, (Asian) Arial, 12 pt, Font color: Text 1, English (UK)

Deleted: ¶

Formatted: Font: (Default) Arial, (Asian) Arial, Font color: Text 1

Formatted: Line spacing: 1,5 lines

Deleted: for

Deleted: the 1980s, and

Deleted: has

Deleted:

Deleted: evolutions

Deleted: about

Deleted:

Deleted: as

Deleted: spars

Deleted: In addition, recent studies (Day et al. 2014; Guemas et al., 2014; Melia et al. 2015) have shown that SIT anomalies play an important role for the Arctic predictability up to seasonal time scale.

Formatted: Font: (Default) Arial, (Asian) Arial, 12 pt, Font color: Text 1, English (UK)

Deleted: Up to the 1990s, the availability of SIT measurement was limited to sparse in situ measurements and submarines

Formatted: Font: (Default) Arial, (Asian) Arial, 12 pt, Font color: Text 1

Deleted: ergence of

Deleted: from the satellites

Deleted: the sea-ice thickness

Deleted: The retrieved

Deleted: still contains considerable uncertainty

Deleted: s

Deleted: for example when estimating

Deleted: These uncertainties

Deleted: comparatively

148 (<1 m). In parallel, satellite measurements from a passive microwave
 149 radiometer have retrieved SIT of thin ice (Martin et al., 2004; Heygster et al.,
 150 2009) from the Soil Moisture and Ocean Salinity (SMOS) satellite brightness
 151 temperature in the L-Band microwave frequency (1.4 GHz) (Kaleschke et al.,
 152 2010; Tian-Kunze et al., 2014). Although the consistency between the SMOS
 153 and CryoSat-2 estimates is still poor (X. Wang et al., 2016), a recent initiative
 154 has combined the two data sets in the Arctic (e.g. Kaleschke et al., 2015; Ricker
 155 et al., 2017) into a merged weekly SIT from the CryoSat-2 altimeter and SMOS
 156 radiometer (referred to as CS2SMOS, available online at
 157 <http://www.meereisportal.de>), The usefulness of assimilating this data set for
 158 reanalysis and operational forecasting needs to be tested.
 159 In this study, the CS2SMOS will be assimilated into the TOPAZ4 forecast
 160 system, which is a coupled ocean-sea ice data assimilation system using the
 161 Deterministic Ensemble Kalman Filter (DEnKF; Sakov and Oke, 2008). The
 162 Ensemble Kalman Filter has previously been demonstrated for assimilation of
 163 SIT data (Lisæter et al., 2007) of freeboard data (Mathiot et al., 2012) and of
 164 the CS2SMOS data (Mu et al., 2018) as well. TOPAZ4 is the Arctic Marine
 165 Forecasting system in the Copernicus Marine Environment Monitoring Services
 166 (CMEMS, <http://marine.copernicus.eu>). Every day, it publishes a 10-day
 167 forecast of the ocean physics and biogeochemistry in the Arctic, through the
 168 CMEMS portal. It also provides a long reanalysis from 1990 to the present –
 169 currently 2016 - that is extended every year. This reanalysis has been widely
 170 used and validated (Ferreira et al., 2015; Johannessen et al., 2014; Xie et al.,
 171 2017). Although SIT products are so far not assimilated into the TOPAZ4
 172 reanalysis, the Arctic SIT distribution in TOPAZ4 shows some degree of spatial
 173 coherency with that of ICESat in spring and autumn of 2003-2008; it
 174 underestimates SIT (up to 1 m) north of Canadian Arctic Archipelago and
 175 Greenland and overestimates it by approximately 0.2 m in the Beaufort Sea
 176 (Xie et al., 2017). Even though the SIT from ICESat has been reported too thick
 177 by about 0.5 m (Lindsay and Schweiger, 2015), the SIT from TOPAZ4
 178 undoubtedly has spatial biases. Similar biases for SIT have been reported for
 179 other Arctic coupled ocean-ice models (Stark et al., 2008; Johnson et al., 2012;
 180 Schweiger et al., 2012; Yang et al., 2014; Smith et al., 2015, Q. Wang et al.
 181 2016) and even reanalyses (Uotila et al., 2018). Xie et al. (2016) have tested

Deleted: b

Deleted: A

Deleted: measurements in Arctic

Deleted:) is now

Deleted: (Ricker et al., 2017)

Deleted: There is a need to test

Deleted: ion of

Deleted: 2007) or f

Deleted: or

Deleted:)

Formatted: Font: (Default) Arial, (Asian) Arial, 12 pt, Font color: Text 1, (Asian) Chinese (China)

Deleted: main

Deleted: rovides

Deleted: stry in the Arctic region

Deleted: for the public

Deleted: hat

Deleted: By default, SIT products are not assimilated into the TOPAZ4 reanalysis.

Formatted: Font: (Default) Arial, (Asian) Arial, 12 pt, Font color: Text 1, English (UK)

Deleted: ,

Deleted: a

201 assimilation of thin SIT (<0.4 m) from SMOS, and show that the assimilation
 202 slightly reduced the SIT overestimation near the sea ice edge. The recent
 203 availability of the weekly SIT from CS2SMOS provides an opportunity for the
 204 TOPAZ4 to constrain better the SIT error in the Arctic. This study aims at
 205 identifying a suitable practical implementation for assimilating C2SMOS data
 206 set and assess its usefulness for the Arctic reanalysis. Although it is expected
 207 that a better initialisation of SIT anomalies will enhance the predictability of the
 208 system, this is beyond the scope of this paper. A similar assessment over the
 209 same time frame has been carried out in the Arctic Cap Nowcast/Forecast
 210 System (ACNFS) by Allard et al. (2018) revealing significant improvements of
 211 bias and RMSD but little changes in ice velocity except in marginal seas. The
 212 proposed study in complementary to Allard et al. (2018) because the TOPAZ4
 213 prediction system uses a more rudimentary sea ice thermodynamics (no explicit
 214 ice thickness distribution) but a more advanced ensemble-based data
 215 assimilation method (TOPAZ4 uses strongly coupled data assimilation of ocean
 216 and sea ice, meaning that sea ice observation will impact also the ocean and
 217 vice versa with a flow dependent assimilation method, see Penny et al., 2017;
 218 Kimmitz et al., 2018).

Deleted: SIT overestimation near the sea ice edge. The recent availability of the weekly SIT from CS2SMOS provides an opportunity for the TOPAZ4 to constrain

Deleted: comparatively

Deleted: -

Deleted: -

Deleted: M

Deleted: (Penny et al., 2017; Kimmitz et al., 2018) -

219 Section 2 describes the TOPAZ4 system: namely the coupled ocean and sea
 220 ice model, the implementation of the EnKF and the observations used for data
 221 assimilation and validation. In section 3, we carry an Observing System
 222 Experiment (OSE) comparing the two reanalyses: one using the standard
 223 observation types used in operational setting and another assimilating the
 224 CS2SMOS in addition. Then the performance of the two runs is presented
 225 against both assimilated and non-assimilated measurements. Section 4
 226 presents the impacts of assimilating the CS2SMOS on sea ice drift and the
 227 integrated quantities for sea ice, and measures its relative impact compared to
 228 other assimilated observations. A summary is provided in the last Section.

Deleted: quantifies

Formatted: Font: (Default) Arial, (Asian) Arial, 12 pt, Font color: Text 1, English (UK)

Deleted:

Deleted: compared to the other ob

Deleted: variable

Deleted: and discussion are

Formatted: Line spacing: 1,5 lines

Deleted: early of

Deleted: initially at University of Miami, which has been successfully applied in global and regional oceans (Chassignet et al., 2003; Counillon and Bertino, 2009; Metzger et al 2014; Xie et al., 2018). Th

2. TOPAZ4 system descriptions and observations

2.1 The coupled ocean and sea-ice model

232 TOPAZ4 is a forecasting ocean and sea-ice system developed for the Arctic,
 233 having been operational since the early 2000s (Bertino and Lisæter, 2008). It
 234 uses the Hybrid Coordinate Ocean Model (HYCOM: version 2.2) developed at

254 University of Miami, which has been successfully applied in global and regional
 255 oceans (Chassignet et al., 2003; Counillon and Bertino, 2009; Metzger et al
 256 2014; Xie et al., 2018). The model grid is constructed using conformal mapping
 257 (Bentsen et al., 1999) with a 12-16 km resolution shown in Fig. 1 (left). The
 258 model uses 28 hybrid layers with reference potential densities selected
 259 specifically for the North Atlantic and the Arctic regions (Sakov et al. 2012). The
 260 model is forced by atmospheric forcing from ERA-Interim. A barotropic inflow
 261 of Pacific Water is imposed through the Bering Strait, which is balanced by an
 262 outgoing flow through the southern model boundary. It has an averaged
 263 transport of 0.8 Sv, and varies seasonally with a minimum (0.4 Sv) in January
 264 and a maximum (1.3 Sv) in June consistently with observations (Woodgate et
 265 al. 2005). The model accounts for river discharge, for which a seasonal
 266 climatology is estimated by feeding the run off from ERA-interim (Dee et al.,
 267 2011) into the Total Runoff Integrating Pathways model (TRIP, Oki and Sud,
 268 1998) over the period 1989–2009.

269 A simple sea ice model using a one-thickness category has been coupled to
 270 HYCOM. The sea ice and the ocean are thus coupled every 3 hours and
 271 exchange momentum, salt and heat on the ocean model's Arakawa C-grid. The
 272 sea ice thermodynamics treat precipitations on ice as snow whenever surface
 273 air temperature is below zero (Drange and Simonsen, 1996). The ice dynamics
 274 uses the elastic-viscous-plastic rheology (Hunke and Dukowicz, 1997) with the
 275 modification suggested by Bouillon et al. (2013). There is a 0.1 m limit in the
 276 model for the minimum thickness of both new ice and melting ice.

2.2 Implementation of the EnKF in the TOPAZ4 system

279 The TOPAZ4 system uses a deterministic Ensemble Kalman Filter (DEnKF,
 280 Sakov and Oke, 2008), which solves the analysis without the need to perturb
 281 the observations and is therefore a square-root filter implementation of the
 282 EnKF. In the DEnKF, if the model state is represented by \mathbf{x} , the ensemble mean
 283 is updated by equation:

$$\mathbf{x}^a = \mathbf{x}^f + \mathbf{K}(\mathbf{y} - \mathbf{H}\mathbf{x}^f), \quad (1)$$

285 where the superscripts "f" and "a" refer respectively to the forecast and the
 286 analysis. Following Xie et al. (2017), the model state vector \mathbf{x} contains 3-

Formatted: Font: (Asian) Times New Roman, English (UK)

Deleted: e model grids are

Deleted: ; Bertino and Lisæter, 2008

Deleted: outf

Deleted: ing

Deleted: seasonally

Formatted: Font: (Default) Arial, (Asian) Arial, Font color: Text 1, English (US)

Deleted: proposed in Woodgate et al. (

Deleted: the

Formatted: Font: (Default) Arial, Font color: Text 1, English (UK)

Deleted:

Deleted: integrated at NERSC into

Deleted: , the sea ice and the ocean are

Commented [LB1]: Updated

Commented [LB2]: Updated

Deleted: described in Drange and Simonsen (1996) treat precipitations on ice as snow whenever surface air temperature is below zero

Deleted: regarded as

Formatted: Line spacing: 1,5 lines

Deleted: respectively

Formatted: Font: (Default) Arial, (Asian) Arial, Font color: Text 1, English (US)

302 dimensional ocean variables in the native hybrid coordinates (u- and v-
 303 components of the current velocities, temperature, salinity and model layer
 304 thickness), the 2-dimensional ocean variables (u- and v-components of the
 305 barotropic velocities, barotropic pressure, and mixed layer depth) and three sea
 306 ice variables: ice concentration, ice thickness and snow depth. The assimilated
 307 observations are represented by the vector **y without perturbation, and** the
 308 observation operator **H** projects the model variables on the observation space.
 309 The misfit between the model and the observation - the bracket term in Eq. (1),
 310 is **the** innovation. The Kalman gain **K** is calculated by:

$$311 \quad \mathbf{K} = \mathbf{P}^f \mathbf{H}^T [\mathbf{H} \mathbf{P}^f \mathbf{H}^T + \mathbf{R}]^{-1} \quad (2).$$

312 Where **P^f** is the background error covariance matrix, **R** is the observation error
 313 covariance matrix, and the superscript "**T**" denotes a matrix transpose. The
 314 background error covariance is approximated from the ensemble anomalies **A**
 315 (where $\mathbf{A} = \mathbf{X} - \mathbf{x}_N$, $\mathbf{I}_N = [1, \dots, 1]$, N being the ensemble size) as $\mathbf{P} = \frac{\mathbf{A} \mathbf{A}^T}{N-1}$. Here,
 316 **X** denotes the ensemble of model states. The observation errors are assumed
 317 to be uncorrelated (i.e. the matrix **R** is diagonal). While this practical assumption
 318 is not valid for interpolated observations, a diagonal approximation combined
 319 with an inflation of the observation error can make a reasonable approximation
 320 when the error spatial structure is unknown (Stonebridge 2018). A localization
 321 is used in order to reduce the sampling error with a radius of 300 km and a
 322 polynomial tapering function (in a local analysis framework).
 323 The practical implementation of the model and its perturbations follow Sakov et
 324 al. (2012); the model errors include joint perturbations of winds, heat fluxes as
 325 originally recommended by Lisæter et al. (2007). The precipitation perturbation
 326 has however been increased from 30% to 100%, following a log-normal
 327 probability distribution of errors (Finck et al. 2013), which also increased the
 328 spread of ice thickness.

330 2.3 Observations for assimilation and validation

331 The following observations are assimilated sequentially every week in the
 332 TOPAZ4 system (Xie et al. 2017): along-track Sea Level Anomaly; in situ
 333 profiles of temperature and salinity; gridded Operational Sea Surface
 334 Temperature and Sea Ice Analysis (OSTIA) SST; Ocean and Sea Ice Satellite

Commented [FC3]: If you call them tracer, then temp and salinity are also tracers

Deleted: and

Deleted: of y without perturbation

Formatted: Font: (Default) Arial, (Asian) Arial, Bold, Font color: Text 1, English (US)

Deleted: as

Formatted: Font: (Default) Arial, (Asian) Arial, Font color: Text 1, English (US)

Deleted: is the matrix of background error covariance

Formatted: Line spacing: 1,5 lines

Commented [FC4]: Do not put that in Bold otherwise it means it is a matrix.

Deleted: follows

Deleted: ,

Deleted: the

Deleted: being

Deleted:

Deleted: allsome types of

Deleted: it requires the sufficient knowledge about the covariance structure for the observation errors if considering the correlations in **R**. Otherwise, an approximation of the correlated observation error can yield a poor analysis so

Deleted: ¶

To ensure that the sampling error remains small, a

Formatted: Font: (Default) Arial, (Asian) Arial, Font color: Text 1, English (US)

Deleted: (local framework analysis)

Deleted: Gaussian

Formatted: Font: (Default) Arial, (Asian) Arial, Font color: Text 1, English (UK)

Deleted: More details about

Formatted: Font: (Default) Arial, (Asian) Arial, Font color: Text 1, (Asian) Japanese, (Other) English (UK)

Formatted: English (US)

Deleted: t

Deleted: .

Deleted: T

Deleted: was

Formatted: Font: (Default) Arial, (Asian) Arial, Font color: Text 1, English (US)

359 Application Facility (OSI-SAF) sea ice concentration and sea ice drift from
 360 satellite observation (Lavergne et al., 2010). All measurements are retrieved
 361 from [CMEMS, http://marine.copernicus.eu](http://marine.copernicus.eu), and are quality controlled and **high-**
 362 **resolution observations are "superobed": all observations falling within the same**
 363 **grid cell are averaged and the observation uncertainty is reduced accordingly (Sakov et**
 364 **al., 2012). For SST and ice concentration, we only retain the observation on the last**
 365 day of the assimilation cycle. Similarly, **only** the sea ice drifts during the last 2
 366 days of the assimilation cycle are assimilated.

367 The weekly SITs of CS2SMOS were retrieved from
 368 <http://data.meereisportal.de/maps/cs2smos/version3.0/n> **on** the period from
 369 March 2014 to March 2015. This product is gridded with a resolution of
 370 approximately 25 km. The provider uses optimal interpolation to blend the
 371 measurements of CryoSat-2 and SMOS based on their uncertainties and their
 372 spatial covariance. An estimate of the observation error is provided with the
 373 data set but **only** accounts for the errors related to the merging and interpolation
 374 (Ricker et al., 2017). As such, we expect that this observation error is
 375 **underestimated since it** misses both the sensor errors and the model-related
 376 representation errors. In particular the mapping **is** based on a no-bias
 377 assumption and **error estimates do** not account for inconsistencies between the
 378 two satellites, like those reported by [X. Wang et al. \(2016\)](#) and Ricker et al.
 379 (2017). With an EnKF assimilation system, underestimating the observation
 380 error leads to an underestimation of the ensemble spread and makes the
 381 system suboptimal, **leading in the worst case, to system divergence,**
 382 Underestimating the errors of one data type also lessens the impact of the other
 383 assimilated observations since they compete for the control of a finite number
 384 of degrees of freedom. This issue will be addressed in Section 4.3. On the other
 385 hand, Oke and Sakov (2008) showed that the performance of the EnKF does
 386 not degrade much when observation error is overestimated. It is therefore
 387 necessary to increase the observation error to a level at least as high as the
 388 optimal value for the performance of the filter (Desroziers et al., 2005; Karspeck,
 389 2016).

390 In order to estimate the representation error for the SIT observation, we have
 391 performed a preliminary sensitivity assimilation experiment for November 2014.
 392 We used the diagnostics by Desroziers et al. (2005) as an indicative lower limit

Field Code Changed

Formatted: Default Paragraph Font, Font: (Default) Times New Roman, Font color: Auto, English (UK)

Formatted: Default Paragraph Font, Font: (Default) Times New Roman, Font color: Auto, Norwegian Bokmål

Deleted: analysis

Formatted: Default Paragraph Font, Font: (Default) Times New Roman, Font color: Auto

Formatted: Default Paragraph Font, Font: (Default) Times New Roman, Font color: Auto, Norwegian Bokmål

Deleted: superobed – i.e. all observations falling within the same grid cell are averaged and the observation uncertainty is reduced accordingly (Sakov et al., 2012). For SST and ice concentration, we only retain the analysis at

Deleted: from OSI-SAF

Deleted: for

Deleted: the best estimate,

Deleted: it

Deleted: only accounting for a part of the real error

Deleted: and

Deleted: error

Deleted: does

Deleted: b

Deleted: . l

Deleted: , the ensemble spread collapses and the

Deleted: s

411 for the observation error in the TOPAZ4 system based on the misfits to the
 412 CS2SMOS data. Desroziers et al. (2005) estimate the optimal observation error
 413 as the following matrix:

414
$$\tilde{\sigma}_{\text{SIT}}^o = \sqrt{\frac{1}{\mathbf{P}} \sum_{j=1}^p (\mathbf{y}_j - \mathbf{H}\bar{\mathbf{x}}^a)(\mathbf{y}_j - \mathbf{H}\bar{\mathbf{x}}^f)} \quad (3)$$

Field Code Changed

415 where p is number of data assimilation steps in the sensitivity run (here 4), and
 416 \mathbf{y}_j represents the observed SIT from CS2SMOS at the j th assimilation time.
 417 Here, the terms $\bar{\mathbf{x}}^a$ and $\bar{\mathbf{x}}^f$ represent the ensemble mean of the analysis and
 418 forecast states. In Fig. 2, the diagnosed observation errors from Desroziers et
 419 al. (2005) are larger than the mapping error included in CS2SMOS, but still do
 420 not account for biases in the CryoSAT2 and SMOS observations. The
 421 CS2SMOS mapping error is particularly low for sea ice below 0.5 m: about 4
 422 times lower than the uncertainties obtained by error propagation in the SMOS
 423 processing chain (used in Xie et al. 2016), which would make the assimilation
 424 of SMOS SIT too strong. The Desroziers diagnosed errors gradually increase
 425 with ice thickness, although they vary unrealistically for SITs above 3 m,
 426 possibly due to low counts of either modelled or observed ice thickness in
 427 certain thickness ranges. In view of the above considerations, we have added
 428 a cautious correction term to the CS2SMOS mapping error estimate, which
 429 simply increases linearly with the observed SIT.

430
$$\epsilon_{\text{Offset}} = \min(0.5, 0.1 + 0.15 * \mathbf{d}_{\text{SIT}}) \quad (4),$$

431 where \mathbf{d}_{SIT} is the observed sea ice thickness. At low SIT, the resulting values
 432 are slightly higher than those used in Xie et al. (2016) and comparable to the
 433 Desroziers diagnostics. At SITs of 1.5 m, for which SMOS and CS2SMOS
 434 overlap, the added correction is comparable to reported differences between
 435 the two satellites: about 20 cm in the Beaufort Sea and 1 meter in the Barents
 436 Sea, see Table 3 in Ricker et al. (2017). Tilling et al., (2018) show that the
 437 standard deviations between the CryoSat-2 and independent measurements
 438 are between 30 and 70 cm depending of the source of observation and increase
 439 with ice thickness (their Figure 16). It should be noted however that the
 440 processing of CryoSat2 data differs in CPOM and AWI's algorithms. The total
 441 observation error including the added term is shown with blue-squared line in

442 Fig. 2. In the following, we will only use the corrected observation error for the
 443 CS2SMOS SIT.

444

445 3. Observing system experiment runs and validations

446 3.1 Experiment and independent observations for validation

447 A parallel OSE is conducted from 19th March 2014 until end of March 2015. The
 448 two assimilation runs cover two special time periods: the onset of ice melting in
 449 March-April 2014 following by a data period **free** of CS2SMOS, **then** a whole
 450 cold season from October 2014 to March 2015. The control run named the
 451 **Official run** uses the standard observational network in the TOPAZ4 system
 452 (Xie et al. 2017), which assimilates on a weekly cycle the SLA, SST, in situ
 453 profiles of temperature and salinity, SIC and sea ice drift (SID) data. Another
 454 assimilation run named the **Test run** **includes as well** the SIT from CS2SMOS.
 455 We discard the SIT closer than 30 km from the coast to account for differences
 456 of coastlines between the model and observations. The innovation of SIT in Eq.
 457 (1) is calculated in terms of sea ice volume:

$$458 \quad \Delta \text{SIT} = \mathbf{d}_{\text{SIT}} - \mathbf{H}(\mathbf{h} \times \mathbf{f})_m \quad (5)$$

459 where \mathbf{d}_{SIT} is the observed SIT from CS2SMOS as in Eq. (4), $(\mathbf{h} \times \mathbf{f})_m$ is the
 460 ensemble mean of ice volumes forecasted by model. The f and h are SIC and
 461 ice thickness within the grid cell respectively. We assume the observation error
 462 is uncorrelated (\mathbf{R} in Eq. (2) is diagonal). Although the minimal thickness in the
 463 model is set to 0.1 m, the ensemble mean from 100 model members can be as
 464 thin as 1 mm, so that we **only** reject the observed SIT if it is equal to 0. Every
 465 week, the SITs from CS2SMOS are considered to be at the analysis time,
 466 neglecting the time delay. The associated errors due to the sea ice motions or
 467 thermodynamic growth/melt of sea ice within one week **remain small** compared
 468 to the large SIT biases targeted in the present exercise.

469 In the following, we investigate the misfits of the forecasted model states by
 470 evaluating the bias and the root mean square difference (RMSD):

$$471 \quad \text{Bias} = \frac{1}{L} \sum_{i=1}^L (\mathbf{H}_i \mathbf{x}_i^f - y_i) \quad (6)$$

$$472 \quad \text{RMSD} = \sqrt{\frac{1}{L} \sum_{i=1}^L (\mathbf{H}_i \mathbf{x}_i^f - y_i)^2} \quad (7).$$

Deleted: at

Deleted: free

Deleted: M

Deleted: and

Deleted: Both runs are forced by atmosphere forcing from ERA-Interim.

Deleted: involves

Deleted: as a type of additional observation into the system

Deleted: The CS2SMOS ice thickness data are weekly averages and provided on a grid with a 25 km resolution.

Deleted: t

Deleted: (

Deleted: $\times f_m$)

Deleted: f

Formatted: English (US)

Formatted: English (US)

Formatted: English (US)

Deleted: SIC, and \mathbf{h}_m is the ensemble mean ice thickness

Deleted: within the grid cell

Deleted: to be

Deleted: While it is clear that this approximation is incorrect, it was shown in Stonebridge et al. (2018) that when the structure of the correlation is unknown, it was best to assume \mathbf{R} diagonal and to tune the inflation.

Deleted: for CS2SMOS only

Deleted: However, t

Deleted: remain small

Deleted: will

501 Where L is the total number of assimilation cycles during the study, \mathbf{x}_i^f is the
502 ensemble mean model state at the i th time, which is compared to the
503 observations \mathbf{y}_i .

504 Three types of independent SIT observations are used for validation. First, the
505 drifting Ice Mass Balance buoys (IMB: [http://imb-crrel-](http://imb-crrel-dartmouth.org/imb-crrel/buoysum.htm)
506 [dartmouth.org/imb-crrel/buoysum.htm](http://imb-crrel-dartmouth.org/imb-crrel/buoysum.htm), Perovich and Richter-Menge, 2006).

507 Four IMB buoys are available during the experimental time period (2013F,
508 2014B, 2014C, and 2014F) and their trajectories are shown in Fig.1 (left).

509 Second, three upward looking sonar (ULS) buoys funded by the Beaufort Gyre
510 Exploration Project (BGEP, see <http://www.whoi.edu/beaufortgyre>) have been
511 moored in the Beaufort Sea. Their locations are shown with the red squares in

512 Fig. 1 (left). They estimate the sea ice drafts since October 2014. Third, the
513 NASA IceBridge Sea Ice Thickness Quick Look data

514 (<https://nsidc.org/data/icebridge>) collected in aerial campaigns estimate the SIT
515 in spring (Kurtz et al., 2013) with a better spatial coverage. The locations of the

516 quality-controlled SIT observations from IceBridge for March and April of 2014
517 and 2015, are shown with the yellow squares in Fig. 1 (left).

518

519 3.2 Validation against CS2SMOS and innovation diagnostics

520 The first assimilation time is the 19th March 2014 and the last is the 25th March
521 2015. The monthly SITs from the two OSE runs are compared to CS2SMOS in

522 Fig. 3. The SITs in April 2014 are presented for comparison in the upper panels
523 of Fig. 3. In the Official run, the thick sea ice to the north of the CAA is

524 underestimated but thickens slightly in the Test run: the 3 m SIT isoline covers
525 a wider area, in better agreement with the observations. The areas of thinner

526 sea ice north of the Barents Sea, west of the Kara Sea, and the coast of the
527 Beaufort Sea, which were too thick in the Official run, have all been improved

528 also shown by reduced area delimited by the isolines of 1 m or 2 m SIT in the
529 Test run.

530 After summer of 2014, measurements of SIT from CS2SMOS restart at the end
531 of October. Results are presented for November 2014 in Fig. 3: the thick sea

532 ice in the central Arctic has been further improved in the Test run. The thickest
533 sea ice (> 3 m) is located near the northern coast of Canada instead of north of

Deleted: over

Deleted: period

Deleted: mean of the model

Deleted: able

Deleted: for SIT

Deleted: involved

Deleted: SIT measurements from

Field Code Changed

Deleted:) buoys (

Formatted: Font: (Default) Arial

Deleted: (2013F, 2014B, 2014C, and 2014F)

Formatted: Font: (Default) Arial

Deleted:

Deleted: s

Deleted: sea ice thickness

Deleted: of SIT

Deleted: on

Deleted: on

Deleted: for

550 Greenland in the Official run. The averaged SIT in the Test run around the North
551 pole (>80°N), is increased from 1.3 m in the Official run to 1.6 m, which is closer
552 to CS2SMOS by 43%. In the marginal zones ~~the~~ East Siberian Sea, Laptev Sea,
553 and Kara Sea, ~~the~~ SITs in the Official run is too thin, but is thicker, in the Test
554 run. Improvements in marginal seas are due to the contribution of SMOS, while
555 improvements in the ice pack are more likely due to CryoSat-2.
556 In the last month of the experimental period (March 2015), the thick sea ice
557 pattern in the Test run, shown as the 2 m isoline, is more similar to CS2SMOS.
558 The maximal SIT within the 4 m isoline is located north of the CAA in the Test
559 run and in CS2SMOS, while in the Official run it spreads further out from the
560 northern coast of Canada to north of Greenland. In addition, the SIT north of
561 the Fram Strait is thicker than in the Official run. The SIT is similarly improved
562 near the coast of the Beaufort Sea and to the northwest of Svalbard. As
563 expected with data assimilation, the Test run agrees clearly better with the
564 assimilated product. Those improvements are largest in the ice pack and in the
565 marginal Seas, where the model deviates considerably from the CS2SMOS
566 SITs. On the contrary, the thickness near the sea ice edge is not strongly
567 impacted by the assimilation.
568 The above results are confirmed quantitatively by comparing misfits of weekly
569 SIT from the two runs with the corresponding CS2SMOS observations. Time
570 series of bias and RMSD calculated as in Eq. (6-7) are shown in the top panel
571 of Fig. 4. In the beginning of the period, the SIT RMSD in the Test run decreases
572 quickly from 0.6 m to 0.4 m before the observations are interrupted for the
573 summer. The biases are reduced equally in both runs. After the observations
574 resume in the end of October 2014, the SIT RMSD is comparable between the
575 two runs but the bias is slightly lower in the Test run. There is large spike in the
576 bias and RMSD for both systems that relates to an inaccuracy of the CS2SMOS
577 observations (see Section 4.2). After the spike, the RMSD and bias in the Test
578 run are lower than in the Official run. The bias in the Test run converges to 0
579 and fluctuates around that level but this is probably not due to the assimilation
580 since the bias in the Official run also converges to 0 during that time. This is
581 rather due to the compensation of seasonal and regional errors. On average,
582 the SIT bias (too thin) is decreased from 15 cm to 5 cm by the assimilation of

Deleted: of the

Deleted: the

Deleted: the

Deleted: ,

Deleted: ned

Deleted: mainly

Deleted: that of

Deleted: denoted by

Deleted: it

Deleted: improves

Deleted: the agreement

Deleted: has a

Deleted: e

Deleted: deviation compared to

Deleted: continuous agreement is

Deleted: :

Deleted: are compared

Deleted: (

Deleted: weekly

Deleted: At

Deleted: of the two runs

Deleted: similarly

Deleted: reduced

Deleted: likely not

Deleted: the influence from

Deleted: as

Deleted: of SIT

610 CS2SMOS. The RMSD of SIT is 38 cm in the Test run, which corresponds to a
611 reduction of 28.3% relative to the error in the Official run.

612 The innovation statistics taken at each assimilation time are used to evaluate
613 how well our data assimilation system is calibrated. In the reliability budget of
614 Rodwell et al. (2016), the total uncertainty of an ensemble data assimilation
615 system is calculated as follows:

$$616 \quad \sigma_{diag} = \sqrt{Bias^2 + \sigma_{en}^2 + \sigma_o^2} \quad , \quad (8).$$

617 where the *Bias* term – i.e. the mean innovation (shown as blue-circled lines) -
618 is calculated as in Eq. (6) at a given assimilation time step, while σ_{en} and
619 σ_o represent respectively the ensemble spread and the standard deviation of
620 the observation errors at the same assimilation time. If the data assimilation
621 system is reliable, the diagnosed total uncertainty should be close to the RMSD,
622 formulated in Eq. (7). Fig. 4 shows that the pink and red lines are evolving
623 reasonably in phase but that the diagnosed error σ_{diag} is twice larger than the
624 RMSD, meaning that our system is overdispersive. The error budget shows that
625 the observation error (σ_o) itself is too large, suggesting that the offset term in
626 Eq. (4) is overestimated, which we do not expect as a serious problem as
627 explained above.

628 The innovation statistics for SIC are mostly identical in the two runs (not shown),
629 the mean misfits for SIC vary around $\pm 4\%$ and are most of the time lower than
630 12%, which is consistent with the evaluation of the TOPAZ4 reanalysis in Xie
631 et al. (2017). It is somewhat disappointing that improvements of ice thickness
632 do not yield visible benefit to ice concentration, but on the other hand a
633 degradation could also have been possible in case the thermodynamical model
634 had been over-tuned to an incorrectly simulated thickness. It should also be
635 noted that the innovations statistics of SST and SLA are also indiscernible in
636 the two runs and not shown either.

637 **3.3 Validation against independent SIT observations**

638 **3.3.1 Ice Mass Balance Buoys**

639 Four IMB buoys are available as independent validation of the impact of the
640 assimilation of CS2SMOS. The buoys are drifting in the Canadian ian Basin (Fig.
641 1), and only one buoy (2013F) lasted during the whole experimental time period
642

Deleted: mean

Deleted: and

Deleted: In

Deleted: we can see

Deleted: much

Deleted: if

Formatted: Font: (Default) Arial, (Asian) Arial, Italic, Font color: Text 1

Deleted: a

650 shown (upper panel of Fig. 5). This buoy exhibits the seasonal variability of SIT:
 651 it reaches 1.5 m in spring 2014, decreases down to 1.0 m in September and
 652 rises again to 2 m in March 2015. The seasonal SIT cycle of the Official run
 653 shows excessive seasonal variability, with a thin bias in summer 2014 and a
 654 thick bias during the two winters. In the Test run (shown as the red-dashed line)
 655 the seasonal cycle is dampened and more consistent with the observations.
 656 The bias is still quite large around March-April and remains so even at the end
 657 of the study period. It should be noted that the impact of CS2SMOS seems
 658 largest in summer, when no observations are assimilated. This illustrates the
 659 persistent effects of winter SIT improving the predictability of the summer Arctic
 660 sea ice as shown in Mathiot et al. (2012). When CS2SMOS is assimilated again
 661 in the fall 2014, the Test run initially overestimates slightly the SIT measured at
 662 the buoy compared to the Official run but is slowly improving as the data is
 663 assimilated. The time-averaged SIT RMSD for buoy 2013F is reduced from
 664 0.33 m in the Official run down to 0.25 m in the Test run, a reduction by 24.2%.
 665 Two other buoys (2014B and 2014C) cover the early months of the
 666 experimental period. The two runs are initially biased with a too thick SIT by 0.5
 667 m and 0.2 m compared to 2014B and 2014C. At buoy 2014B, there is a slight
 668 error reduction during the assimilation period that continues beyond the
 669 assimilation window, similarly to buoy 2013F. At buoy 2014C however, although
 670 the error is reduced during the analysis period, the two assimilation runs
 671 converge during the summer. At these three buoys the assimilation corrects the
 672 mean SIT values and the amplitude of the seasonal cycle but has little influence
 673 on the phase of the seasonal cycle.

674 The buoy 2014F covers the last 6 months of the experimental period. At that
 675 buoy, the assimilation seems increase the errors. It should be noted however
 676 that the constant SIT at buoy 2014F seems unlikely or not representative of the
 677 area.

678 3.3.2 The BGEP mooring buoys

679 In order to convert the sea ice draft measured by ULS from the BGEP buoys to
 680 SIT, we used the balance equation as in Tilling et al. (2018):

$$681 \mathbf{d}_{SIT} = \frac{d_i \rho_w - h_s \rho_s}{\rho_i} \quad (9)$$

Deleted: depicts

Deleted: that

Deleted: available

Deleted: indicates

Deleted: thickness to

Deleted: e

Deleted: (

Deleted:)

Deleted: that in

Deleted: of

Deleted: At

Deleted: the beginning, t

Deleted: of

Deleted: For

Deleted: of the error

Deleted: to reduce

Deleted: as for

Deleted: For

Deleted: error increases beyond the analysis as the error in the official run reduces

Deleted: For

Deleted: have

Deleted: For

Deleted: to be

Deleted: ing

Deleted: Initially and as for 2013F at the same time, the initial value of SIT is too large in Test while it is quite reasonable in the Official run. For 2013F it was the consequence of curing the too low bias in September and having a too vigorous SIT increase November. At the start of assimilation, Test shows a clear – albeit too weak – decrease and a slower growth of the ice thickness compared to the Official Run.

Deleted: growth in

Deleted: is

Deleted: weak the area and very different from the buoy 2013F, with an increase from 1.5 m to only 1.6 m in the whole winter. However, the Test Run shows a pronounced decrease of SIT at the start of assimilation, and afterward shows a slower growth of the SIT compared to the Official Run.

Formatted: Font: (Default) Arial, (Asian) Arial, Italic, Font color: Text 1, English (US)

Deleted: introduced

724 where d_{SIT} is the sea ice thickness, d_i is sea ice draft, h_s is snow depth, ρ_i is sea
725 ice density, ρ_s is snow density and ρ_w is seawater density. The above densities
726 are set to 900, 300, and 1000 kg/m³ as in the TOPAZ model. d_i is the sea ice
727 draft measured by ULS at the fixed locations (see Fig. 1). The snow depth is
728 taken from the model daily snow depths, averaging, the two model runs and
729 interpolating at the buoys locations.

730 The SIT time series of the measurement and of the two runs are shown on Fig.
731 6, from October 2014 onwards. The gray error bars depict the daily standard
732 deviation. The data indicates an increasing SIT from around 0.5 m in October
733 2014 to nearly 2 m in March 2015. The observed SIT at mooring 14D shows a
734 very large daily variability from end of October to November 2014, especially
735 compared with that of moorings 14A and 14B.

736 The weekly SITs from CS2SMOS match well the data with RMSDs of 15, 19
737 and 39 cm during the 6 months, which is lower than in the two model runs. Still,
738 the SIT from CS2SMOS overestimates SIT from October 2014 to middle
739 January 2015 compared to the mooring 14B, and between in Oct and Nov of
740 2014 for mooring 14A. The SITs in the Official run are overestimated in all three
741 locations. The SIT RMSDs are 41, 23 and 51 cm respectively compared to SIT
742 measurement from the three moorings. The SITs in the Test run are closer to
743 observations, thanks to the data assimilation of the SIT from CS2SMOS. The
744 SIT RMSDs in the Test run are respective 25, 33 and 36 cm for moorings 14A,
745 B, D. The error is reduced for moorings 14A and 14D compared to the Official
746 run but increases for mooring 14B, mostly due to the initial mismatch between
747 CS2SMOS and the mooring. Similarly to the comparison with IMB buoys,
748 moorings suggests that error of SIT in the Beaufort Sea is reduced by
749 assimilation of CS2SMOS.

751 3.3.3 IceBridge Quick Look

752 Another independent observation of SIT with better spatial coverage is the SIT
753 Quick Look data from airborne instruments during NASA's Operation IceBridge
754 campaign (Kurtz et al., 2013). Those are available via the National Snow and
755 Ice Data Center (NSIDC), albeit for the months of March and April only. Note
756 that the airborne SITs have been reported to be slightly low-biased by about 5

Deleted: three

Deleted: constant

Deleted: of

Deleted: used

Deleted: estimated by

Deleted: the daily

Deleted: ed

Deleted: of

Deleted: ed

Deleted: to

Deleted: 9

Deleted: SIT

Deleted: to close

Deleted: es

Deleted: set

Deleted: a

Deleted: that of BGEP for buoy

Deleted: buoy of

Deleted: BGEP buoys

Deleted: is

Deleted: the observed mooring estimate

Deleted: D

Deleted: Buoys

Deleted: E

Deleted: nicely

Deleted: d

Deleted: caused by

Deleted: BGEP

Deleted: initially

Deleted: what was found

Deleted: to

Deleted: measurements

Deleted: it

Formatted: Font: (Default) Arial, (Asian) Arial, Italic, Font color: Text 1, English (US)

Deleted: They

791 cm compared to in situ measurements (King et al., 2015). Figure 7 shows all
 792 observed SITs (upper-left panel) from IceBridge, collected during March and
 793 April of 2014-2015. All observed SITs are located in the Canadian Basin and
 794 north of Greenland and cover most of the area where sea ice is thicker than 3
 795 m. Thicknesses between 1~3 m are measured in the Beaufort Sea. The two
 796 simulated SITs in the two model runs show systematic differences of SIT (see
 797 upper-right panel of Fig. 7); the Test run SIT has been thinned in the Beaufort
 798 Sea and thickened near the North Pole. On average, the SIT in the Test run is
 799 increased by 0.1 m and by 0.27 m north of 80°N. Fig. 10b shows that the
 800 frequency distributions of SITs at the International Arctic Buoy Program (IABP)
 801 buoys (locations shown to the right of Fig. 1) have been significantly adjusted
 802 between the two runs: The thick sea ice (>2.2 m) becomes more abundant in
 803 the Test run and the relatively thin sea ice (0.5-1.7 m) more abundant in the
 804 Official run. The averaged SIT thus increases from 1.52 m to 1.62 m in the Test
 805 run.

806 The comparisons of the two OSE runs to the IceBridge data are presented in
 807 the bottom panels. The sea ice in the Official run is too thin at the north of the
 808 CAA and north of Greenland, with a deviation larger than 1.5 m. In the Beaufort
 809 Sea on the contrary, the model is too thick by 0.5 to 1 m. This bias is consistent
 810 with that reported in Xie et al. (2017), where the TOPAZ4 reanalysis (Official
 811 run) was compared to ICESat observations in the period 2003-2008. In the Test
 812 run, the biases are slightly reduced by SIT assimilation, mainly in the Beaufort
 813 Sea and north of Greenland, but the reduction is smaller than the remaining
 814 error. On average, the SIT RMSD is 1.05 m, which corresponds to a reduction
 815 of 12.5% compared to that in the Official run.

816 The regression of the SIT observations from IceBridge to the two OSE runs is
 817 shown in Fig. 8. The Test run shows improved linear correlations to the
 818 observation. The offset at the origin is reduced (0.52 m instead of 0.93 m) and
 819 the slope is closer to 1 than in the Official run. The linear correlation in the Test
 820 run is slightly increased as indicated with the square correlation R^2 . There is
 821 still a lot of spread which keeps the correlation on the low side. However, the
 822 model still underestimates the thickest ice observed in IceBridge, with a bias as
 823 high as 2 m.

824

Deleted: s

Deleted: Sea ice with a t

Deleted: is

Deleted: -

Deleted: SIT in

Deleted: pole

Deleted: the location of

Deleted: in

Deleted: from the International Arctic Buoy Program (IABP)

Deleted: SIT deviations of

Deleted: compared

Commented [FC5]: I don't see on which ground you concluded that this suggest that the bias are from bias in thermodynamic and synamic

Deleted: for

Deleted: of

Deleted: m

Deleted: squared

Deleted: that explains why

842 **4. Impact of CS2SMOS in the data assimilation system**

843 The above results and assimilation diagnostics confirm that the SIT misfits can
844 be controlled - to some degree - by assimilation of the CS2SMOS data, without
845 visible degradation of other assimilated variables. To better understand the
846 advantages and the limits of assimilating the merged SIT product, we further
847 evaluate the impact of CS2SMOS in the assimilation system: first the
848 repercussions on other sea ice variables and integrated quantities, and then
849 through a quantitative impact analysis of CS2SMOS relatively to other
850 assimilated observation types.

851 **4.1. Impact on the sea ice drift**

852 The EnKF implemented in TOPAZ4 updates all the variables in the model state
853 vector using flow-dependent multivariate covariances from the ensemble
854 members (Eqs. 1 and 2). The direct assimilation update of ice drift is however
855 short-lived: the ice drift vectors quickly readjust to wind forcing after assimilation,
856 so the ice drift changes are mostly caused by dynamical readjustments, related
857 to the updated ice thickness and ice concentrations. By the first order
858 approximation of the two-dimensional momentum equation (e.g., Hibler 1986;
859 Hunke and Dukowicz, 1997), the drift velocity of sea ice is mainly controlled by
860 1) the interactions of atmosphere-sea ice, 2) the interactions of ocean-sea ice
861 and 3) the internal sea ice forces which can be represented by the stress tensor
862 σ_i . The work of Olason and Notz (2014, thereafter called ON14) shows from
863 observations that ice thickness is the main driver changes of ice drift in winter
864 (December to March), while the concentration is the main driver in summer
865 (June to November) and ice drift may increase independently from
866 concentration of thickness in transition periods due to increasing fracturing.

867 Following the EVP rheology in Hibler (1979), the stress tensor σ_i is forced by a
868 pressure term Q which takes a function of the sea ice thickness and
869 concentration only.

870
$$Q = P^* d_{SIT} \exp(-C_0(1 - A_{SIC})), \quad (10)$$

871 Where C_0 and P^* are empirical constants, d_{SIT} is SIT, and A_{SIC} is sea ice
872 concentration. ON14 thus show that this type of rheology is able to reproduce
873 the changes of ice drift whenever they are related to changes of concentration
874 and thickness, although not the changes during the transition periods. The

Formatted: Space Before: 0 pt, After: 0 pt, Line spacing: 1,5 lines

875 sensitivity of ice drift to ice thickness can be directly adjusted by tuning the value
876 of P^* in Eq. (10) (see for example Docquier et al., 2017). In the TOPAZ4 model,
877 the sea ice dynamics assume a viscous-plastic material with an adjustment
878 mechanism at short timescales by elastic waves (called EVP, Hunke and
879 Dukowicz, 1997). The ice thickness does as well have an influence on the ice
880 concentrations in the summer due to melting, but this influence is limited in
881 TOPAZ4 by the assimilation of ice concentrations. The winter months in the
882 seasonal cycle (see Figure 6 in ON14) indicate that a 10% increase of ice
883 thickness can reduce the ice drift by 9%. Areas of thinner ice are much more
884 sensitive (see Figure 5 in ON14) and therefore the above numbers are subject
885 to possible biases of ice thickness. The sensitivity on seasonal time scales may
886 also differ from the sensitivity on a weekly time scale (that of the TOPAZ4
887 assimilation cycle).

888 The evaluation in Xie et al. (2017) shows the model drift of sea ice is
889 overestimated by 2 km d^{-1} on average on the Arctic with an uncertainty of 5 km
890 d^{-1} . The thickness of thick ice is also too thin, consistently with the too fast drift
891 (Figures 14 and 17 in Xie et al., 2017). So, the assimilation of ice thickness is
892 expected to improve the ice drift by dynamical model adjustment. Figure 9
893 shows monthly differences of the 2-day sea ice drift (SID) compared to the OSI-
894 SAF estimates based on passive microwave data in April 2014, December 2014
895 and February 2015. The SID in the Official run is too fast in the central Arctic
896 where the SIT was found too thin in Fig. 3. Despite of the relatively small
897 assimilation impact of CS2SMOS on the SID, there are improvements across
898 the Arctic in all winter months.

899 The RMSD of sea ice drift speed in two-days trajectories is reduced by about
900 0.1-0.2 km in April 2014 and February 2015 for the whole Arctic, which
901 corresponds to a reduction of less than 5% of the RMSD. However, near the
902 North Pole (north of 80°N), the reduction of drift RMSDs is more important, by
903 about 0.4-0.5 km. In December 2014 and February 2015 it is about 8-9% of the
904 error in the Official run. Near the North Pole the averaged SIT in March 2015
905 (Fig. 3) is about 10% thicker in the Test run than in the Official run. The impact
906 is more important there than in the rest of the Arctic and well in line with the
907 sensitivity found in ON14. Additionally, there is a small reduction of the fast SID
908 bias but in the case of TOPAZ4, such biases are dependent on the tuning of

Formatted: Font: (Default) Arial, (Asian) Arial, 12 pt, Font color: Text 1, (Asian) Chinese (China)

909 the drag coefficients between sea ice and the air or the ocean, which has been
910 optimized for the SIT distribution of the TOPAZ free run. The tuning of the drag
911 coefficient adopted by Rampal et al. (2016) is independent from SIT values
912 since it only uses free-drifting ice for tuning.

913 To evaluate the potential impact of assimilating the SIT from CS2SMOS on the
914 sea ice motion, we further utilize the data set from the IABP buoys which began
915 in 1990s to monitor ice motion throughout the Arctic Ocean. Only trajectories
916 longer than 30 days and reporting more than 5 times per day are used to
917 estimate the daily drift speed of sea ice. To avoid buoys in open water, the
918 observations are selected based on sea ice concentration (>0.15) and ice
919 thickness (>5 cm) at the nearest model grid cell in both runs. Furthermore, the
920 dataset is restricted in the central Arctic, (delimited by a red line in Fig. 1), where
921 water is deeper than 30 m and further away from the coast than 50 km. A total
922 of 151 buoys are left from this selection, which provide 21,793 daily estimates
923 of drift speed.

924 The speed distribution for daily drift of sea ice from IABP is shown by a
925 histogram in Fig. 10a. In the central Arctic, the averaged drift speed is about
926 10.6 km d^{-1} (consistently with Allard et al., 2018) and most speeds (95%) are
927 slower than 24 km d^{-1} . The difference of drift distributions between the two runs
928 is minor compared to the difference to the IABP data. Restricting the analysis
929 to the area North of 80 degrees, the two runs show larger differences in SIT
930 with a Test run about 30 cm thicker (Fig. 10d), the resulting difference in SID in
931 that area is small (0.2 km d^{-1}) and tends to degrade slightly the performance by
932 slowing down the drift speed (Fig. 10c). This is somewhat contradictory to the
933 analysis with OSI-SAF data which indicated a too fast model drift and smaller
934 errors in the Test run. This inconsistency may be due to the poor spatial
935 coverage of the IABP buoys. In Fig. 1 we can see that buoys north of 80°N are
936 mainly found in the Eurasian Basin and sample poorly the region between the
937 Transpolar Drift Stream and the Beaufort Gyre (Sumata et al., 2014), where the
938 SID misfits are largest and where the model drift is too fast. This poor coverage
939 of IABP buoys may as well explain why the SID comparisons in Allard et al.
940 (2018) were inconclusive.

941

942 **4.2 Impact on the sea ice extent and volume in the central Arctic**

943 In Fig. 3, we show that the Arctic SIT has been improved everywhere, the
944 assessment of the sea ice drift is less conclusive but tends to suggest a slight
945 improvement localized in the central Arctic. However, improving the quantitative
946 match with available observations does not necessarily warrant the physical
947 consistency of basin-scale integrated quantities. The impact of CS2SMOS on
948 the Arctic-wide sea ice extent (SIE) and the sea ice volume (SIV) are
949 investigated for the two runs and compared with the estimates from CS2SMOS
950 and OSI-SAF respectively. Due to differences of resolution and land mask
951 (especially important in the Canadian Archipelago), we focus on the central
952 Arctic domain shown as the red line in the right panel of Fig. 1, excluding parts
953 of the marginal seas.

954 Figure 11 shows the time evolutions of SIE and SIV in the two Official and Test
955 runs. Both are calculated by daily averages in the two model runs. The SIE is
956 classically calculated in the area where the SIC is not less than 15% in the
957 Central Arctic. The SIE shows the expected seasonal cycle with the minimum
958 (close to $3 \times 10^6 \text{ km}^2$) in September 2014 and saturates at a maximum value
959 corresponding to the area of the Central Arctic region (around $6 \times 10^6 \text{ km}^2$) from
960 January to March. The timing of the minimum and maximum from the two model
961 runs agree very well with the observed in OSI-SAF and CS2SMOS (using the
962 weekly concentration from the CS2SMOS product). We can also notice the
963 impact of the weekly assimilation cycle that causes some “sawtooth”
964 discontinuity and indicates that the model tends to both melt too fast in August
965 and freeze too fast in September-October. Overall the SIE differences between
966 the two runs (about $8,000 \text{ km}^2$) are indiscernible during the experimental time
967 period.

968 The time evolutions of the SIV in the two runs show larger differences in the
969 lower panel of Fig. 11. The maximum in the Test run is close to $12 \times 10^3 \text{ km}^3$ in
970 April-May of 2014 and again end of March 2015, and the minimum is close to
971 $5 \times 10^3 \text{ km}^3$ in September 2014. On average, the SIV difference in the two OSE
972 runs is about $1,000 \text{ km}^3$, with lower volume in the Official run. Assimilation of
973 the CS2SMOS data yields an annual increase of the SIV by about 8% relative
974 to that in the Official run. The signature of the assimilation cycle is generally
975 less pronounced than on SIE, except in August 2014 due to the SIC updates
976 that are positively correlated to SIT in the summer (as noted in Lisæter et al.,

977 2003). Compared to the observed SIV from the weekly CS2SMOS, the
978 underestimation is significant at beginning of the runs (about $3 \times 10^3 \text{ km}^3$), but
979 corrected by one third through the first month of assimilation of CS2SMOS.
980 When the CS2SMOS data are missing, the gap between the two runs remains
981 constant throughout the summer due to the long memory of winter ice, as
982 previously noted with the assimilation work of ICESat SIT data in Mathiot et al.
983 (2012). After the end of the summer during which no data of CS2SMOS are
984 available, the SIV from the Test run is in better agreement with the first
985 observed SIV from CS2SMOS. This indicates that the TOPAZ4 Official run has
986 underestimated SIV due to the history of the reanalysis but not as a systematic
987 tendency towards a bias state. The SIV estimates from observations
988 occasionally present sudden discontinuities that seem unrealistic for a large
989 integrated quantity such as the SIV of the central Arctic area. These
990 discontinuities are larger than what the data assimilation system would expect
991 based on the assumed observation error statistics given above. But the time
992 series indicate that the EnKF does, as the name indicates, filter out part of the
993 discontinuities so that only the major spike in early November 2014 causes a
994 discontinuity in the Test run. Fig. 12 shows that the spike corresponds to a large
995 homogeneous increase of SIT in all marginal seas between 26th Oct and 2nd
996 Nov 2014, followed by a large decrease in the subsequent week. The weekly
997 SIT innovation on the 2nd Nov reveals that the increase is largest south of the
998 Eurasian Basin and around the Fram Strait. There, the SIT is thinner than 0.3
999 m on the 26th Oct which may suggest that the problem comes from the SIT
1000 measurement from SMOS. Until such inconsistencies are resolved in the
1001 dataset, we would recommend to either discard the first weeks of observations
1002 or increase the observation error during that period.

1003

1004 **4.3 Quantitative impact for the observational network**

1005 The value of the Degrees of Freedom for Signal (DFS) is commonly used to
1006 monitor the relative impact of different observations in a data assimilation
1007 system (ref. Cardinali et al, 2004; Rodgers 2000; Xie et al, 2018), and is
1008 calculated as follows:

$$1009 \quad \text{DFS} = \text{tr} \left(\frac{\partial \mathbf{y}}{\partial \mathbf{y}} \right) = \text{tr} \left\{ \frac{\partial (\mathbf{H}(\mathbf{x}^3))}{\partial \mathbf{y}} \right\} = \text{tr}(\mathbf{KH}) \quad (11).$$

1010 Where \mathbf{y} is the analyzed observation vector, the observation operator \mathbf{H} is same
 1011 in Eq. (1), and the term tr is the trace operator. The DFS is easily calculated
 1012 and stored while performing the analysis with ensemble data assimilation (see
 1013 Sakov et al. (2012) for an application to the TOPAZ4 system with the EnKF). It
 1014 measures the reduction of uncertainty caused by a given observation type
 1015 expressed as a number of equivalent degrees of freedom. Note that the DFS
 1016 depend on the observation error statistics but not on the actual observation
 1017 values (see equation 11). A DFS of 0 indicates that the observation has no
 1018 impact at all, and a DFS equals to the total number of degrees of freedom
 1019 indicates that the observation has so much impact that it has collapsed the
 1020 ensemble to a single value. As the analysis is solved either in observational
 1021 space or in ensemble space (depending on which is computationally cheapest),
 1022 the DFS cannot exceed the smaller of the ensemble size and the number of
 1023 observations used for the local assimilation. The DFS quantity is linear and can
 1024 be split by observation types and accumulated in time periods. The averaged
 1025 DFS for the k th type of observation can then be noted by \overline{DFS}_k , and thus a
 1026 corresponding Impact Factor (IF) is defined as:

$$1027 \quad IF_k = \frac{\overline{DFS}_k}{\sum_{i=1}^o \overline{DFS}_i} \times 100\% \quad (12).$$

1028 Where o represents the number of different observation types assimilated in
 1029 this time period. IF_k represents the relative impact of the k^{th} type of observations
 1030 with respect to the whole observation network.

1031 Figures 13 and 14 show the IF_k for different observations assimilated in the Test
 1032 run averaged in two typical months: in November 2014 and in March 2015. The
 1033 SIC impacts are dominant close to the sea ice edge and in the CAA region in
 1034 the November, with an average IF of 22.7% in the whole Arctic. The SIT impact
 1035 from CS2SMOS is largest in the central Arctic in November 2014. A relatively
 1036 smaller impact (>20%) is also noticeable in north of the Barents Sea and west
 1037 of the Kara Sea. In the open ocean, the SST and SLA have the largest impact.
 1038 Temperature and salinity profiles have locally an important effect in the ice-
 1039 covered Arctic, where a few of ice-tethered profilers (ITP) are available and the
 1040 uncertainty is large. Xie et al. (2016) applied the same DFS method to evaluate
 1041 the impact of thin SIT from SMOS only. The present results reveal, as expected,
 1042 much larger impacts of CS2SMOS SITs in the central Arctic, with only a few

1043 isolated dips where the ITP profiles are available. The IF is higher where the
1044 ice is thicker, even though the observation error increases as a function of ice
1045 thickness. It indicates that the ensemble background errors increase even more
1046 than the observation errors in thick ice by temporal accumulation of model
1047 errors. For example, errors in precipitation grow as the snow accumulates in
1048 the Fall, and the resulting inter-member variability of snow cover causes inter-
1049 member variability of SIT due to the thermal isolation effect of snow.

1050 In March 2015, CS2SMOS has again a large impact in the central Arctic relative
1051 to other assimilated observations even though previous literature indicates a
1052 lower impact in the midst of winter than when the ice is growing (Mathiot et al.,
1053 2012). The relative IF of SIT indeed remains high even though the absolute
1054 DFS is decreasing, due to the lower impact of other assimilated observations,
1055 in particular SIC (Lisæter et al., 2003). On average, the IF value of CS2SMOS
1056 is about 40%. The high values (>40%) are clearly separated into two areas: one
1057 is to the north of the CAA and Greenland; another following the inner side of
1058 the sea-ice edge in marginal ice zones. The former is primarily a CryoSat-2
1059 contribution, while the latter corresponds to the thin SITs from SMOS. The high
1060 IF in the polar hole is probably undesirable since the observations there are
1061 merely extrapolated, so in the future applications we would recommend
1062 discarding these data, in order to leave the polar hole filled instead with sea ice
1063 advected from areas where trustworthy SIT observations have been
1064 assimilated.

1065

1066 **5. Conclusions and discussions**

1067 CS2SMOS is the first product to monitor the complete pan-Arctic SIT in a
1068 systematic way, although only for the winter months. It is a combination of two
1069 very different, yet very advanced, technologies onboard the SMOS and
1070 CryoSat-2 satellites, calibrated against very few in-situ observations of SIT,
1071 freeboard and snow depths. Altogether, the issue of measurements
1072 uncertainties is particularly delicate for the assimilation of CS2SMOS data. On
1073 the other hand, defining proper model background errors for SIT is just as
1074 delicate, when considering that the simulated SIT accumulates errors both in
1075 the sea ice dynamics (in particular the rheological model) and in the
1076 thermodynamics. The Bayesian approach to confront these two uncertainties is

1077 by Monte Carlo propagation of uncertainties, which is what is practiced in the
1078 present study for the model background error, although not for the observation
1079 error.

1080 This study assesses the impact of assimilating the new SIT product from 19th
1081 March 2014 to 31st March 2015. Compared to the assimilated SIT CS2SMOS,
1082 the thin bias is reduced from 15 cm to 5 cm, and the RMSD also decreased
1083 from 58 cm to 38 cm, a reduction by 28.3%. Other innovation diagnostics show
1084 no degradation towards other assimilated variables –namely SIC, SSH, SST
1085 and TS profiles.

1086 The SIT is also improved when compared to four independent drifting IMB
1087 buoys and three BGEP mooring buoys. The benefits persist throughout the
1088 summer although no SIT observations are available then, consistently with the
1089 experiments from Mathiot et al. (2012). This is important because it suggests
1090 that the model is not attracted to his bias solution. The assimilation reduces the
1091 low SIT biases north of the CAA and north of Greenland and the high bias in
1092 the Beaufort Sea compared to independent observations from Operation
1093 IceBridge. Both the thick pack ice in central Arctic and the thin ice in marginal
1094 seas are corrected. On average, the SIT errors in March- April of 2014 and
1095 2015 are reduced by 15 cm, a reduction by 12.5% compared to the Official run.

1096 The dynamical adjustment following the assimilation of SIT has partially
1097 improved the sea ice drift speeds in the Test run where the SIT has thickened:
1098 the monthly averaged drift speed errors north of 80°N are reduced by 0.4-0.5
1099 km per two days in December 2014 and February 2015 (8-9% reduction of the
1100 error). This has been revealed by satellite products but not IABP in situ buoys
1101 for which the spatial coverage is very poor. However, it should also be reminded
1102 that the drag coefficient used in the Test run were tuned for the Official run
1103 which has a biased SIT. One would expect some improvement with a retuned
1104 drag coefficient value. At term, we consider doing an online parameter
1105 estimation of key parameter such as the drag coefficient as tested in Massonnet
1106 et al. (2014).

1107 In this study, the DFS information in the ensemble data assimilation system has
1108 been applied to quantitatively evaluate the relative contributions of all
1109 assimilated observation types. CS2SMOS has the highest impact near the
1110 northern coast of Canada, north of Greenland, and on the inner side of the sea

1111 ice edge, where the contributions from CryoSat-2 and SMOS SIT were
1112 expected. The results, compared to assimilating SMOS only in Xie et al. (2016),
1113 show the importance of CryoSat-2, particularly in the winter months to constrain
1114 the SIT offsets (also shown by Mu et al. 2018, in a coupled MITgcm model
1115 system) and motivate the assimilation of CS2SMOS in the following reanalysis
1116 of TOPAZ4. However, the impact of SIT observations may vary with the
1117 evaluation of the modelling and observing system. Firstly, the SIC may have
1118 been underestimated in central Arctic due to the simplicity of the present sea
1119 ice model. Further planned developments of TOPAZ include a new model
1120 rheology that is able to resolve the scaling laws of deformation of sea ice
1121 (Rampal et al., 2016) and should therefore improve the background errors of
1122 ice concentration in winter months and sea ice drift, increase the impact of SIC
1123 and SID within the ice pack and reduce the estimated SIT impact accordingly.
1124 Other planned changes such as the simulation of melt ponds are not expected
1125 to influence these results directly since there are no melt ponds when the SIT
1126 data is available. Lastly, if a large number of in situ profiles were available below
1127 the sea ice, they would also compete with the SIT observations.

1128 The above OSE results, like others, are necessarily contingent on adequate
1129 specifications of observation errors. Those are very much simplified in the case
1130 of CS2SMOS, which is not an uncommon case for remote sensing observations:
1131 due to the complexity of the physics involved, the specified observation errors
1132 are reflecting interpolation errors rather than a nonlinear propagation of errors
1133 from their sources (Ricker et al., 2017). In the present study, an offset has been
1134 added to account for this difference in Eq. (4), which results in a conservative
1135 error estimate with respect to the classical Desroziers optimality criterion and a
1136 suboptimal performance in the reliability budget analysis. In the one hand,
1137 reducing the observation would have accelerate the convergence to observed
1138 SIT and converge to a more accurate solution. On the other hand, this would
1139 have made the EnKF less robust to the sudden inconsistencies in the
1140 observations as seen in Fig. 11. Further versions of the CS2SMOS data will
1141 hopefully improve their temporal continuity and the impact of the data can be
1142 increased accordingly.

1143 An alternative to using the scheme CS2SMOS data would have been to
1144 assimilate the two data sets CryoSat-2 and SMOS SIT separately and let the

1145 EnKF merge them together rather than relying on optimal interpolation, as
1146 successfully demonstrated by Mu et al (2018). This would for instance avoid
1147 assimilating observations in places where they are the pure result of
1148 interpolation/extrapolation but would not resolve the offset between the two
1149 satellites, which is arguably the most worrying issue as of the present state of
1150 the SMOS and CryoSat-2 data. The assimilation of the separate datasets will
1151 be attempted in the future when their consistency is further improved.
1152 The current TOPAZ reanalysis is currently reaching 2016 and extended by one
1153 year every year. The current study clearly shows the added value of
1154 assimilating SIT. In 2020, a new TOPAZ reanalysis will be provided with the
1155 upgraded version of TOPAZ5 which will include SIT assimilation from 2010
1156 onwards.

1157

1158 **Acknowledgements**

1159 Thanks to the three anonymous reviewers for constructive comments. Thanks
1160 to Dr. J. A. Johannessen for [discussions](#) and to Dr. S. Hendricks and Dr. R.
1161 Ricker for sharing the CS2SMOS data on meereisportal.de. The authors
1162 acknowledge the support of CMEMS for the Arctic MFC. Grants of computing
1163 time (nn2993k and nn9481k) and storage (ns2993k) from the Norwegian
1164 Sigma2 infrastructures are [also](#) gratefully acknowledged. ▲

1165

1166 **Reference:**

1167 Allard, R. A., Farrell, S. L., Hebert, D. A., Johnston, W. F., Li, L., Kurtz, N. T., Phelps, M.W.,
1168 Posey, P.G., Tilling, R., Ridout, A. Wallcraft, A. J.: Utilizing CryoSat-2 sea ice thickness to
1169 initialize a coupled ice-ocean modeling system. *Advances in Space Research*, 62(6), 1265-
1170 1280, <http://doi.org/10.1016/j.asr.2017.12.030>, 2018.

1171 Bathiany, S., Notz, D., Mauritsen, T., Raedel, G., and Brovkin, V.: On the potential for abrupt
1172 Arctic winter sea ice loss. *J. Climate*, **29**, 2703–2719, <https://doi.org/10.1175/JCLI-D-15-0466.1>, 2016.

1174 Bertino, L., and Lisæter, K. A.: The TOPAZ monitoring and prediction system for the Atlantic
1175 and Arctic Oceans, *Journal of Operational Oceanography*, 1(2), 15–19, doi:
1176 10.1080/1755876X.2008.11020098, 2008

Deleted: nice suggestions

Formatted: Font: (Default) Arial, (Asian) Arial, Italic, Font color: Text 1, English (UK)

1178 Bentsen, M., Evensen, G., Drange, H., and Jenkins, A. D.: Coordinate transformation on a
1179 sphere using conformal mapping, *Mon. Weather Rev.*, 127, 2733-2740,
1180 doi:[http://dx.doi.org/10.1175/1520-0493\(1999\)127<2733:CTOASU>2.0.CO;2](http://dx.doi.org/10.1175/1520-0493(1999)127<2733:CTOASU>2.0.CO;2), 1999.

1181 Bouillon, S., Fichet, T., Legat, V., and Madec, G.: The elastic-viscous-plastic method revised.
1182 *Ocean Modell.*, 7, 2-12, doi:10.1016/j.ocemod.2013.05.013, 2013.

1183 Budikova, D.: Role of Arctic sea ice in global atmospheric circulation: A review. *Global and*
1184 *Planetary Change*, 68,149-163, doi:10.1016/j.gloplacha.2009.04.001, 2009.

1185 Cardinali, C., Pezzulli, S., and Andersson, E.: Influence-matrix diagnostic of a data assimilation
1186 system, *Q. J. R. Meteorol. Soc.*, 130, 2767-2786, doi:10.1256/qj.03.205, 2004.

1187 Chassignet, E. P., Smith, L. T., and Halliwell, G. R.: North Atlantic Simulations with the Hybrid
1188 Coordinate Ocean Model (HYCOM): Impact of the vertical coordinate choice, reference
1189 pressure, and thermobaricity, *J. Phys. Oceanogr.*, 33, 2504-2526. Doi:
1190 [http://dx.doi.org/10.1175/1520-0485\(2003\)033<2504:NASWTH>2.0.CO;2](http://dx.doi.org/10.1175/1520-0485(2003)033<2504:NASWTH>2.0.CO;2), 2003.

1191 Comiso, J. C., Parkinson, C. L., Gersten, R., and Stock, L.: Accelerated decline in the Arctic
1192 sea ice cover. *Geophys. Res. Lett.*, 35, L01703, doi:<https://doi.org/10.1029/2007GL031972>,
1193 2008.

1194 Counillon, F. and Bertino, L.: High-resolution ensemble forecasting for the Gulf of Mexico
1195 eddies and fronts, *Ocean Dynam.*, 59, 83-95, doi:10.1007/s10236-008-0167-0, 2009.

1196 Day, J. J., Hawkins, E., and Tietsche S.: Will Arctic sea ice thickness initialization improve
1197 seasonal forecast skill?, *Geophys. Res. Lett.*, 41, 7566-7575, doi:[10.1002/2014GL061694](https://doi.org/10.1002/2014GL061694),
1198 2014.

1199 Dee, D. P., Uppala, S. M., Simmons, A. J., Berrisford, P., et al.: The ERA-Interim reanalysis:
1200 configuration and performance of the data assimilation system, *Quart. J. Roy. Meteor. Soc.*,
1201 137, 553-597, doi:10.1002/qj.828, 2011

1202 Desroziers, G., Berre, L., and Poli, P.: Diagnosis of observation, background and analysis-error
1203 statistics in observation space. *Q. J. R. Meteorol. Soc.*, 131(613), 3385-3396,
1204 <https://doi.org/10.1256/qj.05.108>, 2005.

1205 Docquier, D., François Massonnet, F., Barthélemy, A., Tandon, N. F., Olivier Lecomte, O., and
1206 Fichet, T.: Relationships between Arctic sea ice drift and strength modelled by NEMO-
1207 LIM3.6. *The Cryosphere*, 11, 2829-2846, <https://doi.org/10.5194/tc-11-2829-2017>, 2017

1208 Drange, H., and Simonsen, K.: Formulation of air-sea fluxes in the ESOP2 version of MICOM,
1209 Technical Report No. 125 of Nansen Environmental and Remote Sensing Center, 1996.

1210 Ferreira, A. S. A., Hátún, H., Counillon, F., Payne, M. R., and Visser, A. W.: Synoptic-scale
1211 analysis of mechanisms driving surface chlorophyll dynamics in the North Atlantic,
1212 *Biogeosciences*, 12, 3641-3653, <https://doi.org/10.5194/bg-12-3641-2015>, 2015.

1213 Finck, N., Counillon, F., Bertino, L., Bouillon, S. and Rampal, P.: Validation of sea ice
1214 quantities of TOPAZ for the period 1990-2010, Technical Report No. 332 of Nansen
1215 Environmental and Remote Sensing Center, 2013.

1216 Guemas, V., Wrigglesworth, E. B., Chevallier, M., et al.: A review on Arctic sea-ice
1217 predictability and prediction on seasonal to decadal time scales. *Q. J. R. Meteorolog. Soc.*,
1218 142(695), 546-561, <https://doi.org/10.1002/qj.2401>, 2014.

1219 Heygster, G., Hendricks, S., Kaleschke, L., Maass, N., et al.: L-Band Radiometry for Sea-Ice
1220 Applications, Final Report for ESA ESTEC Contract 21130/08/NL/EL. Institute of
1221 Environmental Physics, University of Bremen, 219 pages, 2009.

1222 Hibler, W. D., III: A dynamic thermodynamic sea ice model. *J. Phys. Oceanogr.*, **9**, 817–846,
1223 [https://doi.org/10.1175/1520-0485\(1979\)009<0815:ADTSIM>2.0.CO;2](https://doi.org/10.1175/1520-0485(1979)009<0815:ADTSIM>2.0.CO;2), 1979.

1224 Hibler, W. D., III: Ice dynamics. chap. 9, *The Geophysics of Sea Ice*, N. Untersteiner, Ed.,
1225 *NATO ASI Series B: Physics*, Plenum Press, 577–640, 1986.

1226 Hunke, E. C., and Dukowicz, J. K.: An elastic-viscous-plastic model for sea ice dynamics, *J.*
1227 *Phys. Oceanogr.*, **27**, 1849-1867, [https://doi.org/10.1175/1520-](https://doi.org/10.1175/1520-0485(1997)027<1849:AEVPMF>2.0.CO;2)
1228 [0485\(1997\)027<1849:AEVPMF>2.0.CO;2](https://doi.org/10.1175/1520-0485(1997)027<1849:AEVPMF>2.0.CO;2), 1997.

1229 Johannessen, O. M., Shalina, E. V., and Miles, M. W.: Satellite evidence for an Arctic Sea ice
1230 cover in transformation, *Science*, 286, 1937–1939. Doi:10.1126/science.286.5446.1937,
1231 1999.

1232 Johannessen, J. A., et al.: Toward improved estimation of the dynamic topography and ocean
1233 circulation in the high latitude and Arctic Ocean: The importance of GOCE, *Surv. Geophys.*,
1234 35, 661–679, doi:10.1007/s10712-013-9270-y, 2014.

1235 Johnson, M., Proshutinsky A., Aksenov Y., Nguyen A. T., Lindsay R., Haas C., Zhang J.,
1236 Diansky N., Kwok R., et al.: Evaluation of Arctic sea ice thickness simulated by Arctic
1237 Ocean Model Intercomparison Project models. *J. Geophys. Res.*, 117(C8), C00D31,
1238 doi:10.1029/2011JC007257, 2012.

1239 Kaleschke, L., Maaß, N., Haas, C., Hendricks, S., Heygster, G., and Tonbøe, R.: A sea-ice
1240 thickness retrieval model for 1.4 GHz radiometry and application to airborne measurements
1241 over low salinity sea-ice, *The Cryosphere*, 4, 583-592. Doi: 10.5194/tc-4-583-2010, 2010.

1242 Kaleschke, L., Tian-Kunze, X., Maaß, N., Ricker, R., Hendricks, S., and Drusch, M.: Improved
1243 retrieval of sea ice thickness from SMOS and Cryosat-2. Proceedings of 2015 International
1244 Geoscience and Remote Sensing Symposium IGARSS, doi:
1245 10.1109/IGARSS.2015.7327014, 2015.

1246 Karspeck, A. R.: An ensemble approach for the estimation of observational error illustrated for

1247 a nominal 1 global ocean model. *Monthly Weather Review*, 144, 1713-1728, DOI:
1248 10.1175/MWR-D-14-00336.1, 2016.

1249 Kern, S., Khvorostovsky, K., Skourup, H., Rinne, E., Parsakhoo, Z. S., Djepa, V., Wadhams,
1250 P., and Sandven, S.: The impact of snow depth, snow density and ice density on sea ice
1251 thickness retrieval from satellite radar altimetry: results from the ESA-CCI Sea Ice ECV
1252 Project Round Robin Exercise. *The Cryosphere*, 9, 37-52, doi:10.5194/tc-9-37-2015, 2015.

1253 Khvorostovsky, K., and Rampal, P.: On retrieving sea ice freeboard from ICESat laser
1254 altimeter. *The Cryosphere*, 10, 2329-2346, doi:10.5194/tc-10-2329-2016, 2016.

1255 Kimmritz, M., Counillon, F., Bitz, C.M., Massonnet, F., Bethke, I. and Gao, Y., 2018.
1256 Optimising assimilation of sea ice concentration in an Earth system model with a
1257 multicategory sea ice model. *Tellus A: Dynamic Meteorology and Oceanography*, 70(1),
1258 1435945, <https://doi.org/10.1080/1600870.2018.1435945>, 2018.

1259 King, J., Howell, S., Derksen, C., Rutter, N., Toose, P., Beckers, J. F., Haas, C., Kurtz, N., and
1260 Richter-Menge, J.: Evaluation of Operation IceBridge quick-look snow depth estimates on
1261 sea ice, *Geophys. Res. Lett.*, 42, 9302–9310, doi:10.1002/2015GL066389, 2015.

1262 King, J., Skourup, H., Hvidegaard, S. M., Rösel, A., Gerland, S., Spreen, G., . . . Liston, G. E.
1263 (2018). Comparison of freeboard retrieval and ice thickness calculation from ALS,
1264 ASIRAS, and CryoSat-2 in the Norwegian Arctic to field measurements made during the
1265 N-ICE2015 expedition. *Journal of Geophysical Research: Oceans*, 123, 1123–1141.
1266 <https://doi.org/10.1002/2017JC013233>

1267 Kinnard, C., Zdanowicz, C. M., Fisher, D. A., Isaksson, E., Vernal, A., and Thompson, L.
1268 G.: Reconstructed changes in Arctic sea ice over the past 1,450 years. *Nature*, 479, 509–
1269 512. doi:10.1038/nature10581, 2011.

1270 Kwok, R., and Rothrock, D.: Decline in Arctic sea ice thickness from submarine and ICESat
1271 records: 1958–2008, *Geophys. Res. Lett.*, 36, L15501, doi:10.1029/2009GL039035, 2009.

1272 Kurtz, N. T., Farrell, S. L., Studinger, M., Galin, N., Harbeck, J. P., Lindsay, R., Onana, V. D.,
1273 Panzer, B., and Sonntag, J. G.: Sea ice thickness, freeboard, and snow depth products from
1274 Operation IceBridge airborne data, *The Cryosphere*, 7, 1035-1056, doi:10.5194/tc-7-1035-
1275 2013, 2013.

1276 Laxon, S., Peacock, N., and Smith, D.: High interannual variability of sea ice thickness in the
1277 Arctic region, *Nature*, 425, 947-950, doi:10.1038/nature02050, 2003.

1278 Lavergne, T., Eastwood, S., Teffah, Z., Schyberg, H., and Breivik, L. -A.: Sea ice motion from
1279 low resolution satellite sensors: an alternative method and its validation in the Arctic.
1280 *Journal of Geophysical Research*, 115, C10032, 2010. doi: 10.1029/2009JC005958, 2010.

1281 Levermann, A., Mignot, J., Nawrath, S., Rahmstorf, S.: The role of Northern sea ice cover for
1282 the weakening of the thermohaline circulation under global warming. *J. Climate*, 20, 4160-
1283 4171, <https://doi.org/10.1175/JCLI4232.1>, 2007.

1284 Lindsay, R., and Schweiger, A.: Arctic sea ice thickness loss determined using subsurface,
1285 aircraft, and satellite observations, *The Cryosphere*, 9, 269-283, doi:10.5194/tc-9-269-2015,
1286 2015.

1287 Lisæter, K. A., Rosanova, J. J., and Evensen, G.: Assimilation of ice concentration in a coupled
1288 ice ocean model, using the Ensemble Kalman filter. *Ocean Dynamics*, 53, 368-388,
1289 doi:10.1007/s10236-003-0049-4, 2003.

1290 Lisæter, K. A., Evensen, G., and Laxon, S.: Assimilating synthetic CryoSat sea ice thickness in
1291 a coupled ice-ocean model, *J. Geophys. Res.*, 112, C07023, doi:10.1029/2006JC003786,
1292 2007.

1293 Martin, S., Drucker, R., Kwok, R., and Holt, B.: Estimation of the thin ice thickness and heat
1294 flux for the Chukchi Sea Alaskan coast polynya from Special Sensor Microwave/Imager
1295 data, 1990-2001, *J. Geophys. Res.*, 109, C10012, <https://doi.org/10.1029/2004JC002428>,
1296 2004.

1297 Massonnet, F., Goosse, H., Fichefet, T., and Counillon, F.: Calibration of sea ice dynamic
1298 parameters in an ocean-sea ice model using an ensemble Kalman filter, *J. Geophys. Res.*,
1299 119(7), 4168-4184, <https://doi.org/10.1002/2013JC009705>, 2014.

1300 Mathiot, P., König Beatty, C., Fichefet, T., Goosse, H., Massonnet, F., and Vancoppenolle, M.:
1301 Better constraints on the sea-ice state using global sea-ice data assimilation, *Geosci. Model*
1302 *Dev.*, 5, 1501-1515, <https://doi.org/10.5194/gmd-5-1501-2012>, 2012.

1303 Melia, N., Haines, K., and Hawkins, E.: Improved Arctic sea ice thickness projections using
1304 bias-corrected CMIP5 simulations, *The Cryosphere*, 9, 2237-2251,
1305 <https://doi.org/10.5194/tc-9-2237-2015>, 2015.

1306 Metzger, E. J., Smedstad, O. M., Thoppil, P. G., Hurlburt, H. E., Cummings, J. A., Wallcraft,
1307 A. J., Zamudio, L., Franklin, D. S., Posey, P. G., Phelps, M. W. and Hogan, P. J.: US Navy
1308 operational global ocean and Arctic ice prediction systems. *Oceanography*, 27(3), 32-43,
1309 <https://doi.org/10.5670/oceanog.2014.66>, 2014.

1310 Mu, L., Yang, Q., Losch, M., Losa, S. N., Ricker, R., Nerger, L., and Liang, X.: Improving sea
1311 ice thickness estimates by assimilating CryoSat-2 and SMOS sea ice thickness data
1312 simultaneously. *Q. J. R. Meteorol. Soc.*, 144(711), 529-538, DOI:10.1002/qj.3225, 2018.

1313 Oke, P. R., and Sakov, P.: Representation error of oceanic observations for data assimilation.
1314 *J. Atmos. Oceanic Technol.*, 25, 1004–1017, doi:10.1175/2007JTECHO558.1, 2008.

1315 Oki, T., and Sud, Y. C.: Design of Total Runoff Integrating Pathways (TRIP)—A Global River
 1316 Channel Network. *Earth Interact.*, **2**, 1–37, [https://doi.org/10.1175/1087-](https://doi.org/10.1175/1087-3562(1998)002<0001:DOTRIP>2.3.CO;2)
 1317 [3562\(1998\)002<0001:DOTRIP>2.3.CO;2](https://doi.org/10.1175/1087-3562(1998)002<0001:DOTRIP>2.3.CO;2), 1998.

1318 Olason, E., and Notz, D.: Drivers of variability in Arctic sea-ice drift speed, *J. Geophys. Res.*
 1319 *Oceans*, **119**, 5755–5775, doi:10.1002/2014JC009897, 2014.

1320 Penny, G., Akella, S.R., Frolov, S., Fujii, Y., Karspeck, A., Peña, M., Subramanian, A., Tardif,
 1321 R., Wu, X., Anderson, J., Kalnay, E., Kleist, D.T., and Todling, R.: Coupled Data
 1322 Assimilation for Integrated Earth System Analysis and Prediction : Goals , Challenges , and
 1323 Recommendations. Technical Report, <https://ntrs.nasa.gov/search.jsp?R=20170007430>,
 1324 2017.

1325 Perovich, D. K., and Richter-Menge, J. A.: From points to Poles: extrapolating point
 1326 measurements of sea-ice mass balance. *Ann. Glaciol.*, **44**, 188–192,
 1327 doi:10.3189/172756406781811204, 2006.

1328 Posey, P. G., Metzger, E. J., Wallcraft, A. J., Hebert, D. A., Allard, R. A., Smedstad, O. M.,
 1329 Phelps, M. W., Fetterer, F., Stewart, J. S., Meier, W. N., and Helfrich, S. R.: Improving
 1330 Arctic sea ice edge forecasts by assimilating high horizontal resolution sea ice concentration
 1331 data into the US Navy’s ice forecast systems, *The Cryosphere*, **9**, 1735–1745,
 1332 doi:10.5194/tc-9-1735-2015, 2015.

1333 [Rampal, P., J. Weiss, and D. Marsan, 2009: Positive trend in the mean speed and deformation](#)
 1334 [rate of Arctic sea ice, 1979–2007, *J. Geophys. Res.*, **114**\(C5\), doi:10.1029/2008JC005066.](#)

1335 Rampal, P., Bouillon, S., Ólason, E., and Morlighem, M.: neXtSIM: a new Lagrangian sea ice
 1336 model. *The Cryosphere*, **10**(3), 1055–1073, 2016.

1337 Ricker, R., Hendricks, S., Helm, V., Skourup, H., and Davidson, M., Sensitivity of CryoSat-2
 1338 Arctic sea-ice freeboard and thickness on radar-waveform interpretation, *The Cryosphere*,
 1339 **8**, 1607–1622, doi:10.5194/tc-8-1607-2014, 2014.

1340 Ricker, R., Hendricks, S., Kaleschke, L., Tian-Kunze, X., King, J. and Haas, C.: A weekly
 1341 Arctic sea-ice thickness data record from merged CryoSat-2 and SMOS satellite data, *The*
 1342 *Cryosphere*, **11**, 1607–1623, doi:10.5194/tc-11-1607-2017, 2017.

1343 Rodgers, C.: Inverse methods for atmospheres: theory and practice, World Scientific, 2000.

1344 Rodwell, M. J., Lang, S. T. K., Ingleby, N. B., Bormann, N., Hólm, E., Rabier, F., Richardson,
 1345 D. S. and Yamaguchi, M.: Reliability in ensemble data assimilation. *Quart. J. Roy. Meteor.*
 1346 *Soc.*, **142**, 443–454, doi: 10.1002/qj.2663, 2016.

1347 Sakov, P., and Oke, P. R.: A deterministic formulation of the ensemble Kalman Filter: an
 1348 alternative to ensemble square root filters. *Tellus A*, **60**(2), 361–371, doi:10.1111/j.1600-
 1349 0870.2007.00299.x, 2008.

Formatted: Font: (Default) Times, (Asian) Times, 11 pt, English (US)

Formatted: Line spacing: 1,5 lines

Formatted: Font: (Default) Times, (Asian) Times, 11 pt, Font color: Text 1

1350 Sakov, P., Counillon, F., Bertino, L., Lisæter, K. A., Oke, P. R., and Korablev, A.: TOPAZ4:
1351 an ocean-sea ice data assimilation system for the North Atlantic and Arctic. *Ocean Science*,
1352 8(4), 633–656. <http://doi.org/10.5194/os-8-633-2012>, 2012.

1353 Schofield, O., Ducklow, H. W., Martinson, D. G., Meredith, M. P., Moline, M. A., and Fraser,
1354 W. R.: How Do Polar Marine Ecosystems Respond to Rapid Climate Change? *Science*
1355 (328), 5985, 1520–1523, DOI: 10.1126/science.1185779, 2011.

1356 Schweiger, A., Lindsay, R., Zhang, J., Steels, M., Stern, H., and Kwok, R.: Uncertainty in
1357 modeled Arctic sea ice volume, *J. Geophys. Res.*, 116, C00D06, doi:10.1029/2011JC007084,
1358 2012.

1359 Smith, G. C., Roy, F., Reszka, M., Colan, D. S., He, Z., Deacu, D., et al.: Sea ice forecast
1360 verification in the Canadian Global Ice Ocean Prediction System. *Quart. J. Roy. Meteor.*
1361 *Soc.*, doi:10.1003/qj.2555, 2015.

1362 Stark, J. D., J. Ridley, M. Martin, M., and Hines, A.: Sea ice concentration and motion
1363 assimilation in a sea ice–ocean model, *J. Geophys. Res.*, 113, C05S91,
1364 doi:10.1029/2007JC004224, 2008.

1365 Stonebridge, G., Scott, K. A., and Buehner, M.: Impacts on sea ice analyses from the
1366 assumption of uncorrelated ice thickness observation errors: Experiments using a 1D toy
1367 model, *Tellus A: Dynamic Meteorology and Oceanography*, 70(1), 1445379, DOI:
1368 10.1080/16000870.2018.1445379, 2018.

1369 Stroeve, J. C., Serreze, M. C., Holland, M. M. et al.: The Arctic’s rapidly shrinking sea ice
1370 cover: a research synthesis. *Climatic change*, 10 (3), 1005-1027, doi:10.1007/s10584-011-
1371 0101-1, 2012.

1372 Sumata, H., Lavergne, T., Girard-Ardhuin, F., Kimura, N., Tschudi, M. A., Kauker, F., Karcher,
1373 M., and Gerdes, R.: An intercomparison of Arctic ice drift products to deduce uncertainty
1374 estimates, *J. Geophys. Res. Oceans*, 119, 4887–4921, doi:10.1002/2013JC009724, 2014.

1375 Tian-Kunze, X., Kaleschke, L., Maaß, N., Mäkynen, M., Serra, N., Drusch, M., and Krumpen,
1376 T.: SMOS-derived sea ice thickness: algorithm baseline, product specifications and initial
1377 verification, *The Cryosphere*, 8, 997-1018, doi:10.5194/tc-8-997-2014, 2014.

1378 Tilling, R. L., Ridout, A., and Shepherd, A.: Near real time Arctic sea ice thickness and volume
1379 from CryoSat-2, *The Cryosphere*, 10, 2003-2012, doi:10.5194/tc-10-2003-2016, 2016.

1380 Tilling, R. L., Ridout, A., and Sheperd, A.: Estimating Arctic sea ice thickness and volume
1381 using CryoSat-2 radar altimeter data. *Advances in Space Research*, 62(6), 1203-1225,
1382 <http://doi.org/10.1016/j.asr.2017.10.051>, 2018.

1383 Uotila, P., Goosse, H., Haines, K., Chevallier, M., Barthélemy, A., Bricaud, C., Carton, J.,
1384 Fučkar, N., Garric, G., Iovino, D., Kauker, F., Korhonen, M., Lien, V. S., Marmela, M.,

1385 Massonnet, F., Mignac, D., Peterson, A., Sadikn, R., Shi, L., Tietsche, S., Toyoda, T., Xie,
1386 J., Zhang, Z.: An assessment of ten ocean reanalyses in the polar regions, *Climate Dynamics*,
1387 <https://doi.org/10.1007/s00382-018-4242-z>, 2018.

1388 [Wang, Q., Ilicak, M., Gerdes, R., Drange, H., Aksenov, Y., Bailey, D. A., ..., Yeager, S. G. An](#)
1389 [assessment of the Arctic Ocean in a suite of interannual CORE-II simulations. Part I: Sea](#)
1390 [ice and solid freshwater. *Ocean Modelling*, 99, 110–132.](#)
1391 <http://doi.org/10.1016/J.OCEMOD.2015.12.008>, 2016a

1392 Wang, X., Key, J., Kwok, R., and Zhang, J.: Comparison of Arctic sea ice thickness from
1393 satellites, aircraft, and PIOMAS data. *Remote Sensing*, 8(9), 1–17,
1394 <http://doi.org/10.3390/rs8090713>, 2016b.

1395 Woodgate, R., Aagaard, K. and Weingartner, T.: Monthly temperature, salinity, and transport
1396 variability of the Bering Strait through flow. *Geophys. Res. Lett.*, 32, L04601, DOI:
1397 10.1029/2004GL021880, 2005.

1398 Xie, J., Bertino, L., Counillon, F., Lisæter, K. A., and Sakov, P.: Quality assessment of the
1399 TOPAZ4 reanalysis in the Arctic over the period 1991–2013. *Ocean Science*, 13(1), 123–
1400 144. <http://doi.org/10.5194/os-13-123-2017>, 2017.

1401 Xie, J., Bertino, L., Cardellach, E., Semmling, M., and Wickert, J.: An OSSE evaluation of the
1402 GNSS-R altimetry data for the GEROS-ISS mission as a complement to the existing
1403 observational networks, *Remote Sens. Environ.*, 209, 152–165,
1404 doi:10.1016/j.rse.2018.02.053, 2018.

1405 Xie, J., Counillon, F., Bertino, L., Tian-Kunze, X., and Kaleschke, L.: Benefits of assimilating
1406 thin sea-ice thickness from SMOS into the TOPAZ system. *The Cryosphere*, 10, 2745–2761.
1407 <http://doi.org/10.5194/tc-10-2745-2016>, 2016.

1408 Yang, Q., Losa, S. N., Losch, M., Tian-Kunze, X., Nerger, L., Liu, J., Kaleschke, L., and Zhang,
1409 Z.: Assimilating SMOS sea ice thickness into a coupled ice-ocean model using a local SEIK
1410 filter, *J. Geophys. Res.*, 119, 6680–6692, doi:10.1002/2014JC009963, 2014.

1411

Formatted: Font: (Default) Times, (Asian) Times, 11 pt

Formatted: Font: (Default) Times, (Asian) Times, 11 pt, English (US)

Formatted: Font: (Default) Times, (Asian) Times, 11 pt, Italic, English (US)

Formatted: Font: (Default) Times, (Asian) Times, 11 pt, English (US)

Formatted: Font: (Default) Times, (Asian) Times, 11 pt, Italic, English (US)

Formatted: Font: (Default) Times, (Asian) Times, 11 pt, English (US)

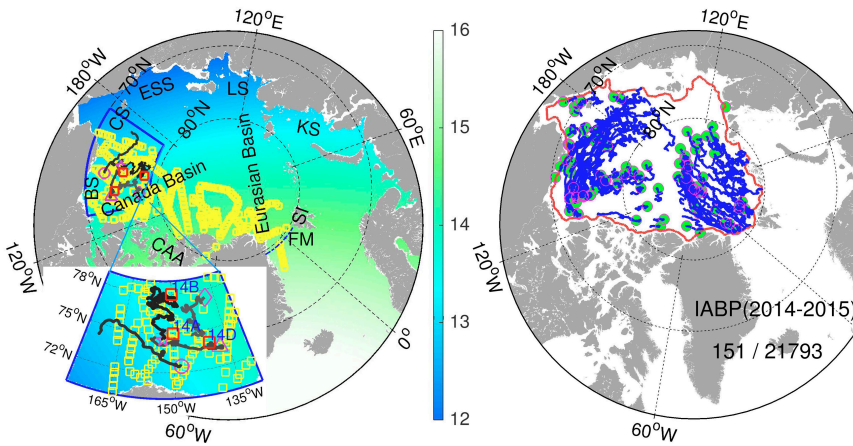
Formatted: Line spacing: 1,5 lines

Formatted: Font: (Default) Times, (Asian) Times, Helvetica, 11 pt, Font color: Text 1, English (US)

1412
1413
1414
1415

Figures:

Formatted: Line spacing: 1,5 lines
Formatted: Font: Arial, 16 pt

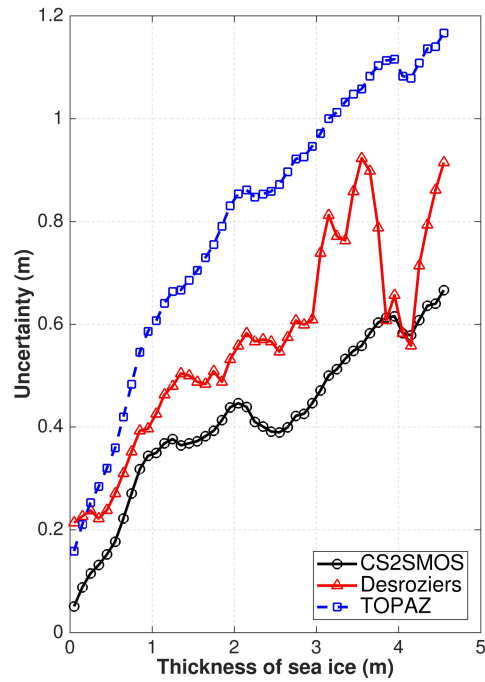


1416
1417
1418
1419
1420
1421
1422
1423
1424
1425
1426
1427
1428
1429
1430
1431
1432
1433

Fig. 1 Left: Horizontal resolution (km) of the model grid in the Arctic (>60°N). The small yellow squares are the locations of IceBridge campaigns during the experimental period. The marginal seas are: Beaufort Sea (BS, ; also shown with the blue line), Chukchi Sea (CS), East Siberian Sea (ESS), Laptev Sea (LS), Kara Sea (KS) and the other regions: Canadian Arctic Archipelago (CAA), Svalbard Island (SI), and Fram Strait (FM). The four purple markers (star, circle, triangle and diamond) are the deployment location of IMB buoys (2013F, 2014B, 2014C, and 2014F respectively) with the following trajectory shown as black solid curves. The three red squares are the fixed locations of the BGEP moorings (14A, 14B, and 14D respectively). **Right:** Trajectories of International Arctic Buoy Program buoys drift during the experimental period. The solid red line delimits the coastal areas excluded in the analysis.

Deleted: pentagram

1435



1436

1437 **Fig. 2** Observation error uncertainties as a function of sea ice thickness for the
1438 original CS2SMOS data set (black line), the estimated observation error using the
1439 Desroziers diagnostics with red-triangle line (see Eq. (3)) and the one used in the
1440 TOPAZ Test run with blue-square, with an additional error term as Eq. (4) to the
1441 original uncertainty.

1442

1443

1444

1445

1446

1447

1448

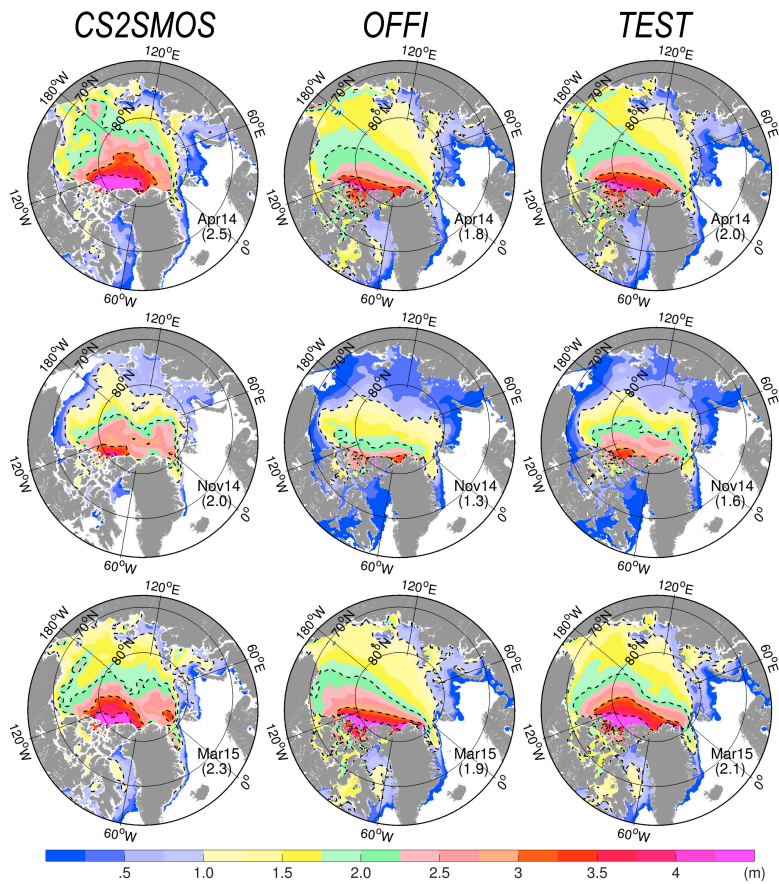
1449

1450

1451

1452

0



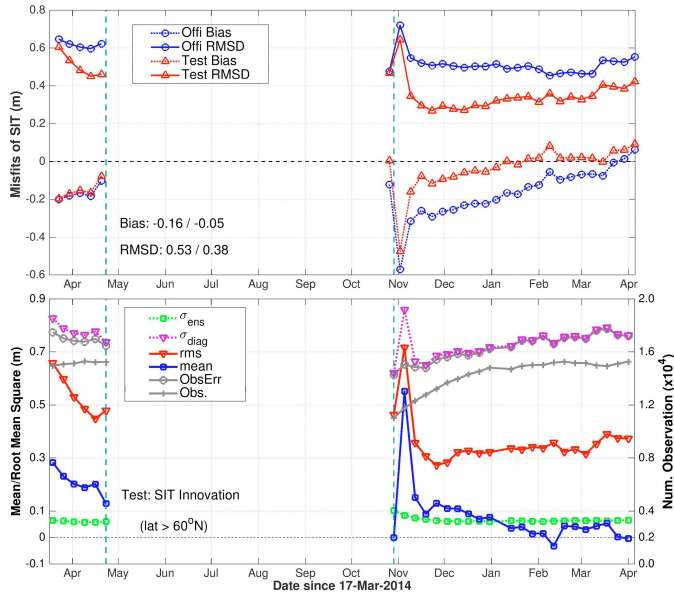
1453
 1454
 1455
 1456
 1457
 1458
 1459
 1460
 1461
 1462
 1463
 1464
 1465

Fig. 3 Monthly SIT from CS2SMOS (left), Official run (middle) and Test run (right) in April 2014, November 2014, and March 2015. The mean SIT estimated for the area north of 80N is indicated in brackets (unit: m). The dashed lines are isolines of 1, 2, 3, and 4 meters SIT respectively.

Formatted: Line spacing: 1,5 lines

Formatted: Font: Arial, Bold, English (US)

1466



1467

1468 **Fig. 4 Top:** Bias (dotted line) and RMSD (solid line) of SIT in the two runs - Official
1469 (blue) and Test (red) – based on weekly averaged reanalysis and CS2SMOS
1470 observations. The time-averaged bias and RMSD are indicated (Official/Test).

1471 **Bottom:** SIT innovation statistics in the Test run in the Arctic region (>60°N) from
1472 19th March 2014 to end of March 2015. The blue-squared (resp. red reverted-triangle)
1473 line represents the mean (RMSD) of the innovation. The green squared line
1474 represents the ensemble spread and the purple reverted-triangle line is the
1475 diagnosed total uncertainty (see Eq. (8)). The gray-crossed (gray-circled) line is the
1476 number (RMSD observation error) of assimilated observations.

1477

1478

1479

1480

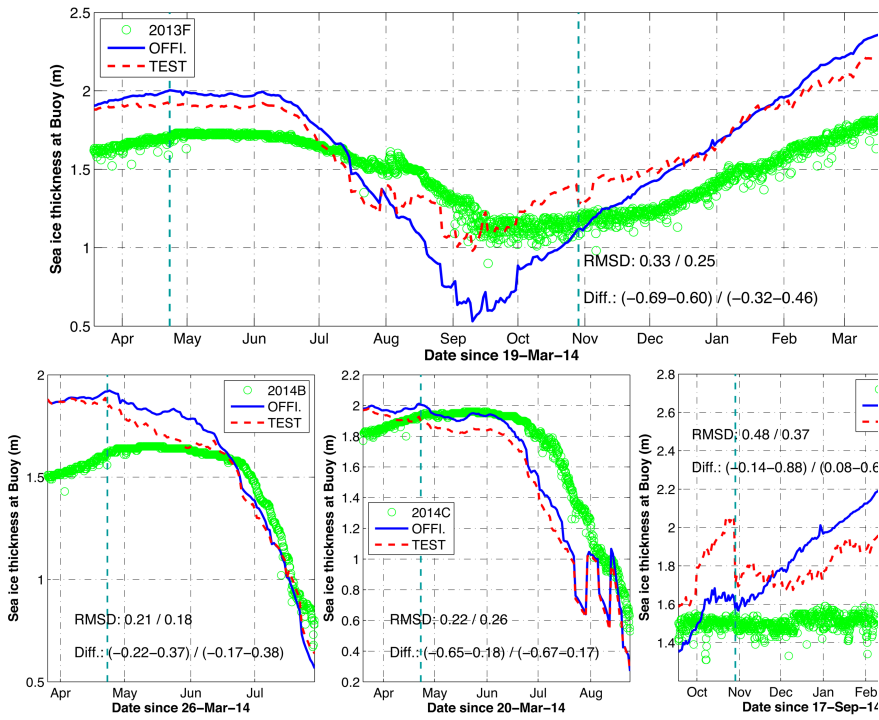
1481

1482

1483

1484

1485



141

1487

1488 **Fig. 5** Time series of SIT along the trajectories of IMB buoys (upper: 2013F; bottom:
 1489 2014B, 2014C, and 2014F). Measured SIT (green), daily averages from the Official
 1490 run (blue line) and the Test run (red line). The vertical cyan-dashed lines indicate
 1491 the winter period when C2SMOS is assimilated in the Test run.

1492

1493

1494

1495

1496

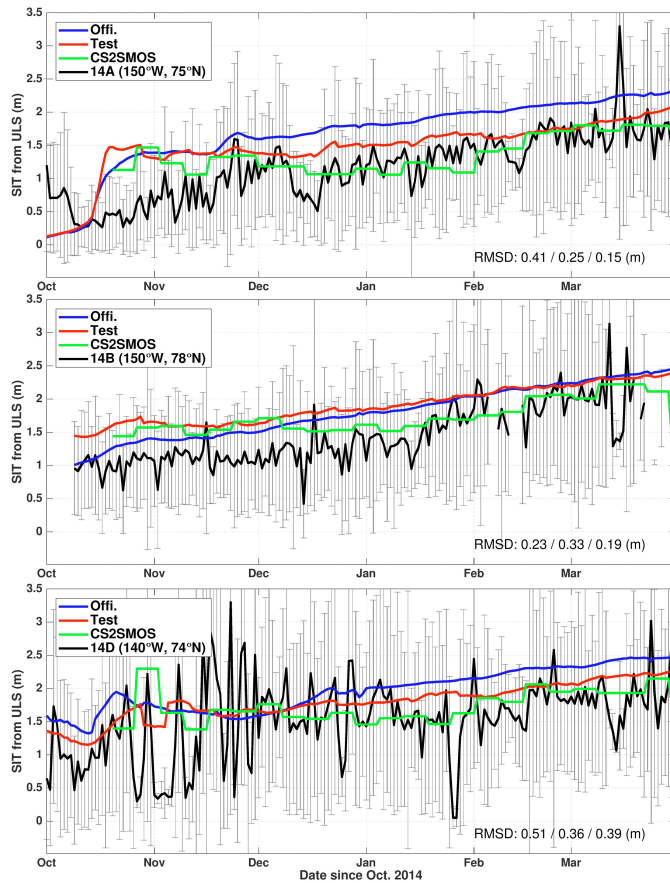
1497

1498

1499

1500

1501



1502

1503 **Fig. 6** Daily series of SIT (black line) at the BGEP mooring (14A, 14B, and 14D)
 1504 compared with the two model runs - Official (blue line) and Test (red line) - and
 1505 the weekly observed by CS2SMOS (green line). The black line represents the
 1506 daily average at the mooring location with the standard deviation shown as the
 1507 error bar. The RMSDs of the Official run, Test run and CS2SMOS are
 1508 respectively indicated on the bottom of each panels.

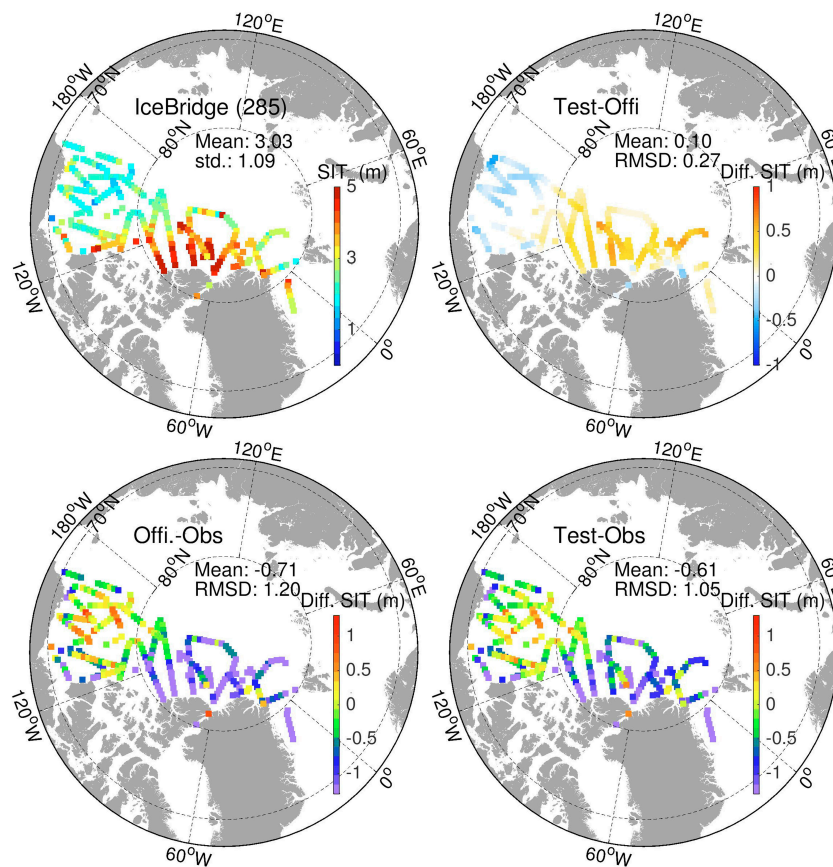
1509

1510

1511

1512

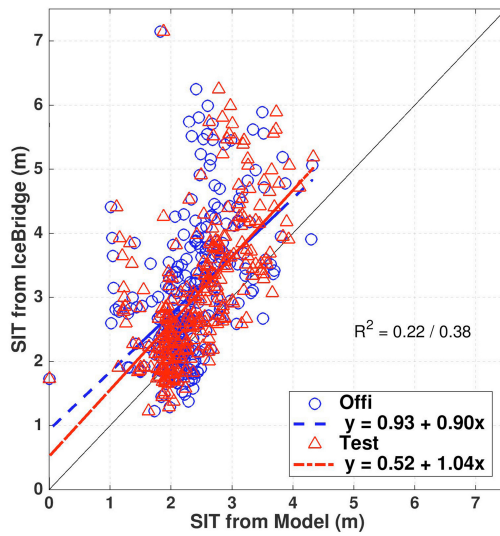
1513



1514
 1515 **Fig. 7 Top:** IceBridge SIT in 2014 and 2015 (left) and the SIT differences in the two
 1516 model runs according to the observational locations and times (right). **Bottom:** SIT
 1517 deviations from the Official run (left) and Test run (right) using model daily average
 1518 at observations time.

1519
 1520
 1521
 1522
 1523
 1524
 1525
 1526

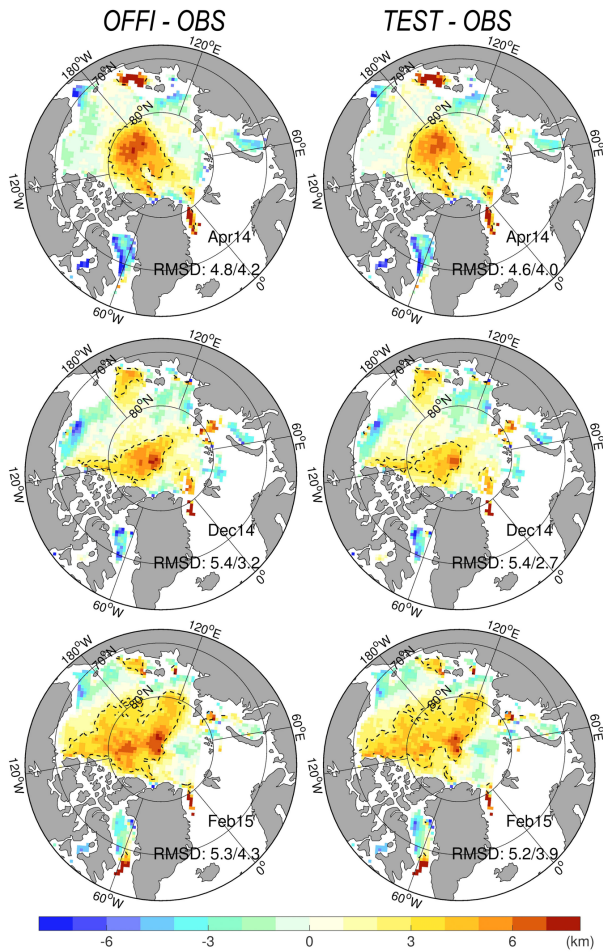
1527
1528
1529
1530
1531



1532
1533
1534
1535
1536
1537
1538
1539
1540
1541
1542
1543
1544
1545
1546
1547

Fig. 8 Scatterplots of SIT daily averaged of Official (blue) and Test (red) runs compared to IceBridge data. The dashed lines are the respective linear regression, the coefficient R^2 is the squared correlation to represent how strong of the linear relationship in Official/Test run. The black line is $y=x$.

1548



1549

1550

1551

1552

1553

1554

1555

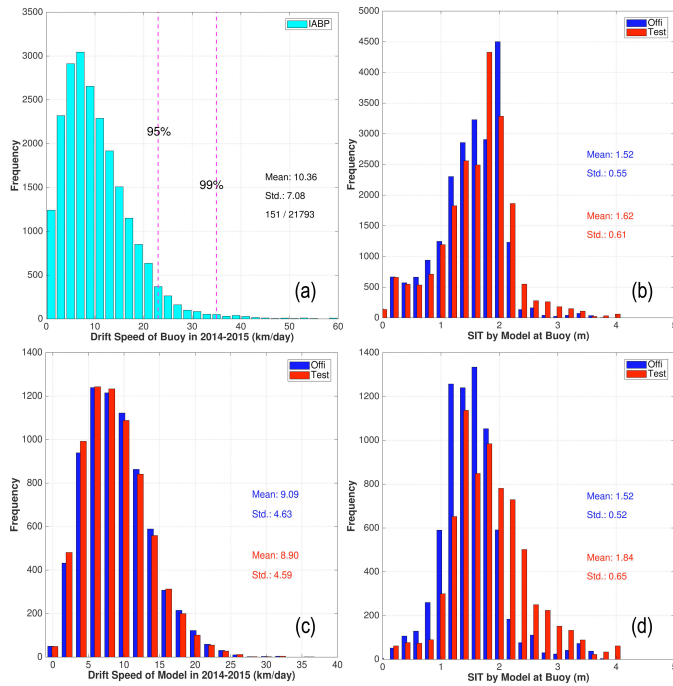
1556

1557

1558

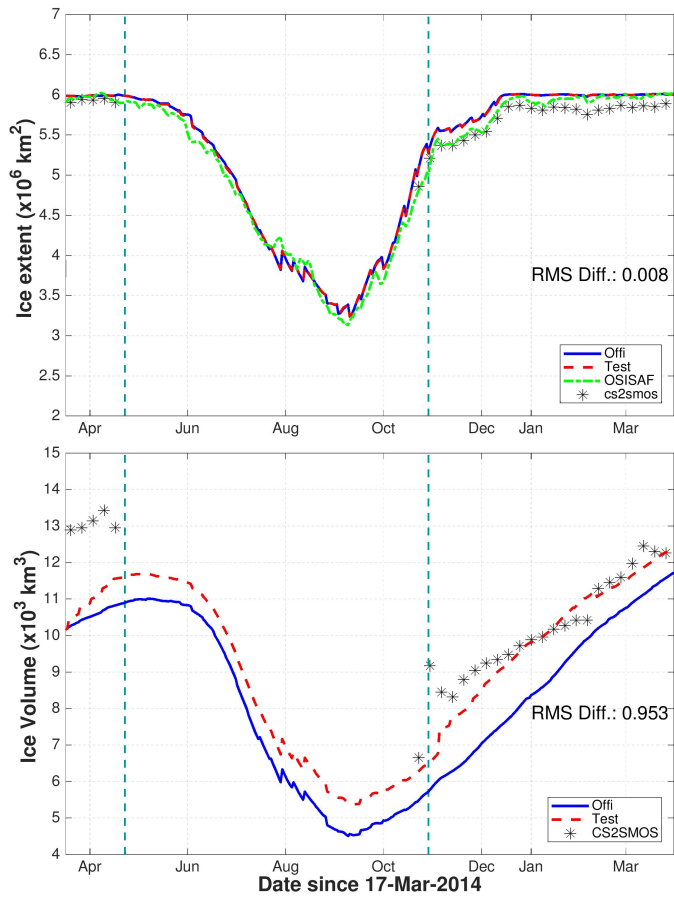
Fig. 9 Sea ice drift misfits (model minus observation, in km per two days) in the Official run (left column) and Test run (right column) compared against the OSI-SAF sea ice drift in April 2014 (top line), December 2014 (middle line), and February 2015 (bottom line). The black dashed delimits the area of fastest drift (drift > 3km per 2 days), and the RMSD relative to the monthly observations is indicated when calculated for the whole domain and at for the region north of 80°N.

1559
1560



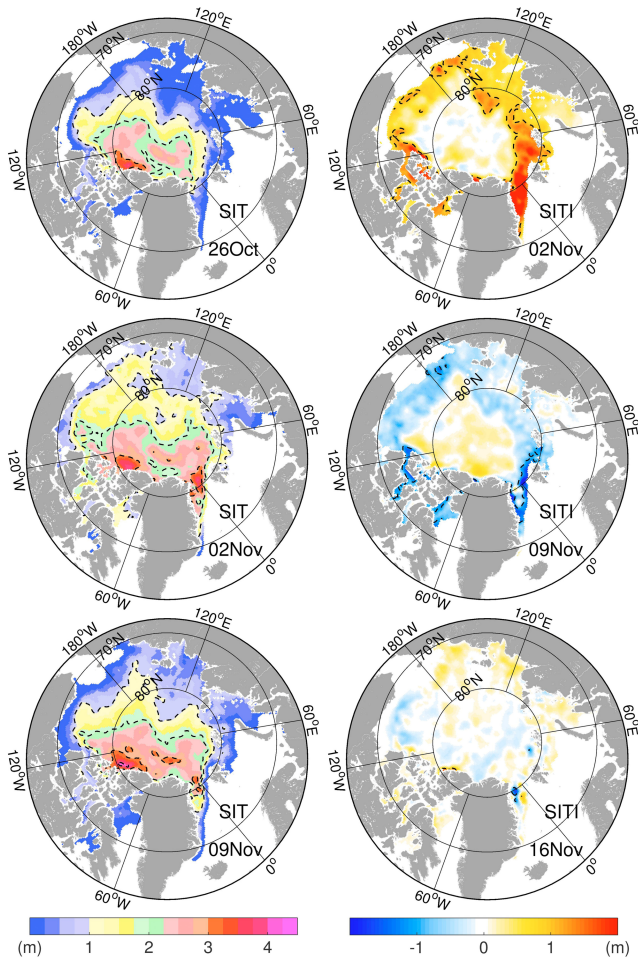
1561
1562
1563
1564
1565
1566
1567
1568
1569
1570

Fig. 10 (a) Histogram of sea ice drift speeds calculated from IABP buoys in the central Arctic for the period 2014-2015. (b) histogram of the simulated SIT at buoys locations in the central Arctic from the two runs. (c) histogram of the drift speed restricted near the North pole (>80°N) in the Official (blue) and Test (red) runs; the mean speed and the standard deviation are indicated; (d) histogram of the simulated SIT near the North pole from the two runs;



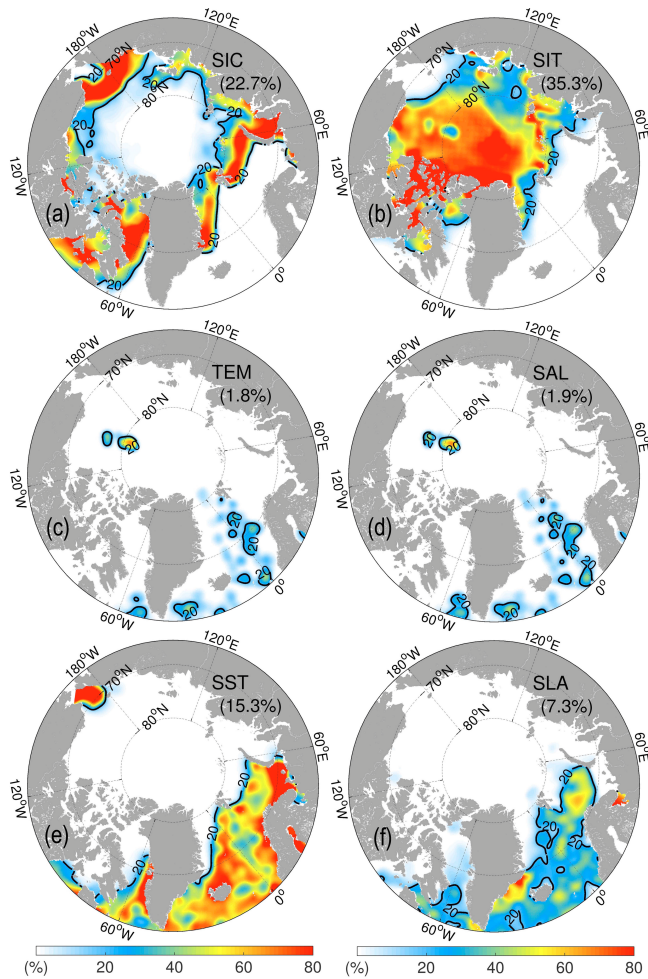
1571
 1572 **Fig. 11** SIE and SIV in the official run (blue) and the test run (red) in the Central
 1573 Arctic. The black stars are the corresponding weekly SIE (or SIV) estimated from
 1574 CS2SMOS. The green dash-dotted line is the daily SIE from OSI-SAF. The
 1575 averaged differences of the two runs (Official-Test) are reported. The vertical cyan-
 1576 dashes delimits the periods when C2SMOS data is assimilated.

1577
 1578
 1579
 1580
 1581
 1582



1583
 1584
 1585
 1586
 1587
 1588
 1589
 1590
 1591
 1592

Fig. 12 Left: First three weekly SITs (20th-26th Oct; 27th Oct-2nd Nov; 3rd-9th Nov) from CS2SMOS in the beginning of fall 2014. The dashed white lines denote the 1, 2, 3, and 4 m isolines. **Right:** The associated time increments of SIT relative to the last weekly SIT. The dashed lines denote the -1 and 1 m isolines.



1593

1594 **Fig. 13** Relative DFS contributions (IF) of each observation data types in November
 1595 2014. (a) SIC from OSI-SAF; (b) SIT from CS2SMOS; (c) temperature profiles; (d)
 1596 salinity profiles; (e) SST; (f) along-track sea level anomaly (SLA). The black line is
 1597 the 20% isoline, and the monthly IF (see Eq. 15) is reported between parenthesis.

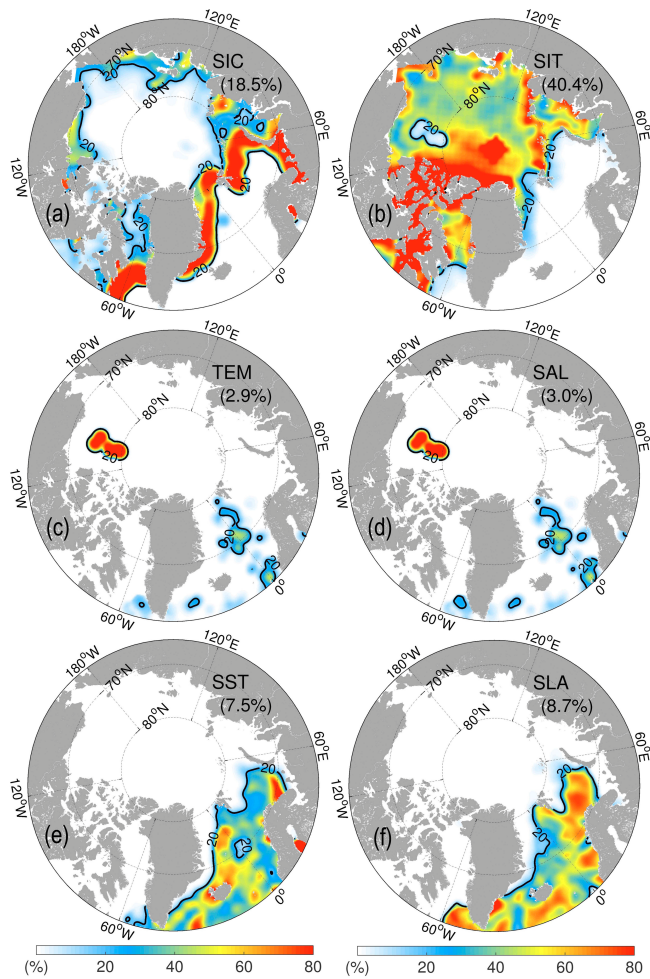
1598

1599

1600

1601

1602



1603

1604 **Fig. 14** Same as the above but for March 2015.

1605

1606

1607